The Malawi Active Fault Database: an onshore-offshore database for regional assessment of seismic hazard and tectonic evolution

Jack N. Williams[1,2], Luke N. J. Wedmore[2], Christopher A Scholz[3], Folarin Kolawole[4], Lachlan J. M. Wright[3], Donna J Shillington[5], Åke Fagereng[1], Juliet Biggs[2], Hassan Mdala[5], Zuze Dulanya[6], Felix Mphepo[5], Patrick Chindandali[8], Maximilian J. Werner[2]

[1]*School of Environmental Sciences, Cardiff University, Cardiff, UK*

[2]*School of Earth Sciences, University of Bristol, Bristol, UK*

[3]*Department of Earth Sciences, Syracuse University, Syracuse, New York, USA*

[4]*BP America, Houston, Texas, U.S.*

[5]*School of Earth and Sustainability, Northern Arizona University, Flagstaff, Arizona, USA*

[6]*Geological Survey Department, Mzuzu Regional Office, Mzuzu, Malawi*

[7]*Geography and Earth Sciences Department, University of Malawi, Zomba, Malawi*

[8]*Geological Survey Department, Zomba, Malawi*

Key points

- Digital elevation models, offshore seismic reflection surveys, and aeromagnetic data are synthesized to identify active faults in Malawi.
- Mapped faults are incorporated into the Malawi Active Fault Database (MAFD), a geospatial database for seismic hazard assessment.
- Active faults greater than 50 km-long are found throughout Malawi, and the distribution of their lengths follows a power law.

Abstract

We present the Malawi Active Fault Database (MAFD), a geospatial database of 114 active fault traces in Malawi, and in neighboring Tanzania and Mozambique. The MAFD has been developed from a multidisciplinary dataset: high resolution digital elevation models, field observations, aeromagnetic and gravity data, and seismic reflection surveys from offshore Lake Malawi. Active faults longer than 50 km are found throughout Malawi, where seismic risk is increasing due to its rapidly growing population and its seismically vulnerable building stock. The MAFD also provides an opportunity to investigate the population of normal faults in an incipient continental rift. We find that the null hypothesis that the distribution of fault lengths in the MAFD is described by a power law cannot be rejected. Furthermore, a power-law distribution of faults in Malawi is consistent with its thick seismogenic crust (~35 km), and low (<8%) regional extensional strain that is predominantly (50-75%) accommodated across relatively long hard-linked border faults. Cumulatively, the data and inferences drawn from the MAFD highlight the importance of integrating onshore and offshore geological and geophysical data to develop active fault databases along the East African Rift and similar continental settings, both to understand the regional seismic hazard and tectonic evolution.

Plain Language Summary

Earthquakes represent the phenomena of incremental slip along cracks in the Earth’s crust. Therefore, mapping these cracks, or ‘faults,’ is important when assessing seismic hazard. However, faults are challenging to identify as they may not propagate to the Earth’s surface, are buried by younger geological units, or are located offshore. In this study, we describe how we identified faults in Malawi, which is located along the tectonically active East African Rift (EAR). Specifically, offshore faults under Lake Malawi were mapped using acoustic images of sediments under the lake from seismic reflection surveys. Buried faults were identified from aeromagnetic data, which detect variations in the spatial distribution of magnetic minerals in the Earth's crust. Faults identified from these surveys were then combined with faults exposed at the surface into the Malawi Active Fault Database (MAFD), a freely available geospatial database. We suggest that the MAFD will be useful for seismic hazard planning in Malawi, where population growth and seismically vulnerable building stock are increasing seismic risk. We also find that fault lengths in the MAFD follow a power law distribution. This suggests that a small number of relatively long (>100 km) faults accommodate most of the EAR extension in Malawi.

1. Introduction

Systematically mapping active faults and collating their geomorphic attributes into an active fault database provides an important tool for assessing regional seismic hazard and tectonic evolution [*Faure Walker et al.*, 2021; *Langridge et al.*, 2016; *Styron & Pagani*, 2020; *Williams et al.*, 2021]. In particular, there is a critical need to develop active fault databases along the Western Branch of the East African Rift (EAR) where population growth and seismically-vulnerable building stock are raising seismic risks [*Goda et al.*, 2016; *Novelli et al.*, 2019]. Due to the paucity of active fault data, previous Probabilistic Seismic Hazard Analysis (PSHA) in the EAR has typically only considered the instrumental record of earthquakes [*Midzi et al.*, 1999; *Poggi et al.*, 2017]. However, this record is short (~70 years) relative to the fault recurrence intervals implied by low regional extension rates [~0.5-3 mm/yr; *Saria et al.*, 2014; *Stamps et al.*, 2018, 2020; *Wedmore et al.*,*in review*], and so only a limited understanding of the magnitude and frequency of earthquakes in the EAR can be incorporated into PSHA [*Hodge et al.*, 2015; *Williams et al.*, 2021].

The Western Branch of the EAR has accommodated relatively small regional extensional strains [<15%; *Scholz et al.*, 2020; *Wright et al.*, 2020], and so active fault databases in this region can also be used to investigate normal fault populations at an early stage of continental rift evolution. In particular, fault lengths in continental rifts are commonly thought to evolve from a power law to exponential distribution with increasing regional extensional strain (>8-12%) as relatively short faults link together or become inactive [*Cowie et al.*, 1995; *Gupta & Scholz*, 2000; *Hardacre & Cowie*, 2003; *Meyer et al.*, 2002; *Michas et al.*, 2015]. However, this transition may be affected by pre-existing crustal heterogeneities and the thickness of the seismogenic crust [*Ackermann et al.*, 2001; *Hardacre & Cowie*, 2003; *Soliva & Schulz*, 2008; *Walsh et al.*, 2002]. Active fault databases in the EAR Western Branch can place constraints on how these factors influence normal fault populations because: (1) faults in this region have inherited mechanical weakness imparted by successive Proterozoic orogenic events [*Kolawole et al.*, 2018a; *Ring*, 1994; *Versfelt & Rosendahl*, 1989], and (2) amagmatic sections of the rift are hosted in relatively thick (20-40 km) seismogenic crust [*e.g. Craig & Jackson*, 2021; *Ebinger et al.*, 2019; *Foster & Jackson*, 1998; *Lavayssière et al.*, 2019; *Nyblade & Langston*, 1995] compared to the seismogenic layer in typical continental crust [~10-20 km thick; e.g. *Jackson et al.*, 2021].

Many challenges exist in locating and mapping active faults because of processes such as scarp degradation, sedimentation, or because faults are buried or offshore

[*Avouac*, 1993; *Nicol et al.*, 2016; *Wallace*, 1980]. These challenges are particularly pertinent in the EAR Western Branch. For example, the relatively thick seismogenic crust means that active faults are less likely to propagate to the surface; as demonstrated by M_W >6 earthquakes in East Africa with large focal depths (>20 km) and no surface expression [*Gupta*, 1992; *Jackson & Blenkinsop*, 1993; *Kolawole et al.*, 2017]. Furthermore, except for a handful of local studies [*Delvaux et al.*, 2017; *Vittori et al.*, 1997], very little chronostratigraphic data exists in the EAR Western Branch to help determine which faults are active.

Extension in the EAR Western Branch combined with a favorable hydroclimate has also resulted in the formation of several rift-axial lakes that have flooded the rift valleys and obscured surface traces of active faults (Figure 1). In active fault databases from other offshore regions, seismic reflection and/or high resolution (spatial accuracy <1 m) bathymetric data have been used to identify and map offshore active faults [*Gràcia et al.*, 2003; *Langridge et al.*, 2016; *Marlow et al.*, 2000; *Pondard & Barnes*, 2010; *Styron et al.*, 2020]. Modern, precision bathymetric data are not available for the lakes in the EAR and although many of the lakes are covered by seismic reflection surveys [*Karp et al.*, 2012; *McGlue et al.*, 2006; *Muirhead et al.*, 2019; *Scholz et al.*, 2020], faults identified in these surveys are not typically incorporated into seismic hazard assessment. Furthermore, even in other regions with well-developed active fault maps, the coverage of offshore data is often incomplete and the information associated with offshore active faults is limited [*Field et al.*, 2014; *Langridge et al.*, 2016; *Styron et al.*, 2020]. Nevertheless, the inclusion of offshore faults into active fault databases is critical as in addition to ground shaking, they also present secondary seismic hazards such as earthquake triggered landslides and near-field tsunamis [*Bardet et al.*, 2003; *Masson et al.*, 2006].

In this study, we present the Malawi Active Fault Database (MAFD), which we have developed in an effort to address the challenges of mapping active faults in the Western Branch of the EAR. The MAFD combines offshore active faults below Lake Malawi, which were mapped from available 2D seismic reflection surveys [*Scholz et al.*, 2020; *Shillington et al.*, 2020], with onshore active faults identified from high resolution digital elevation models [*Hodge et al.*, 2019; *Wedmore et al.*, 2020a; *Williams et al.*, 2021] and faults with no surface expression, but that are identified in aeromagnetic [*Kolawole et al.*, 2018a, 2021] or gravity data [*Chisenga et al.*, 2019].

Except for the Kivu Rift [*Delvaux et al.*, 2017] onshore-offshore active fault databases have not been developed within the Western Branch. The strategies employed to identify and map active faults in the MAFD are therefore relevant elsewhere along the rift system and in other regions with onshore and offshore active faults. Furthermore, the systematic compilation of 114 active fault traces in the MAFD provides a dataset to assess the population of normal faults in a low-strain continental rift that follows pre-existing crustal weaknesses and is hosted in thick seismogenic crust.

2. Malawi Seismotectonics

Malawi is located near the southern end of the Western Branch of the East African Rift (EAR), where the rift accommodates 0.5-2 mm/yr ENE-WSW extension between the San and Rovuma plates [Figure 1; *Wedmore et al.*, in review]. The EAR in Malawi has mainly developed within Proterozoic greenschist to granulite facies metamorphic terranes that bound Archean cratons (Figure 2), and that formed and evolved during the incremental assemblage of the African continent [*Fritz et al.*, 2013; *Lenoir et al.*, 1994; *Manda et al.*, 2019; *Ring*, 1993]. Cumulatively, these events imparted gently to steeply dipping NE to NW striking metamorphic fabrics, which are well-oriented for reactivation under the region's ENE trending minimum principal compressive stress [σ_3; *Dawson et al.*, 2018; *Kolawole et al.*, 2018a; *Ring*, 1994; *Scholz et al.*, 2020; *Wedmore et al.*, 2020b; *Williams et al.*, 2019]. In addition to these relatively high metamorphic grade terranes and structures, the EAR cuts across several NE-SW trending basins in central and northern Malawi that formed during subsequent Upper Permian to Lower Jurassic 'Karoo' rifting event [Figure 2; *Accardo et al.*, 2018; *Key et al.*, 2007; *Ring*, 1994; *Wopfner*, 2002]. In southern Malawi, Karoo-age structures in the NW-SE trending Shire Rift Zone have been reactivated during EAR deformation [Figure 2; *Castaing*, 1991; *Habgood*, 1963; *Kolawole et al.*, 2021; *Wedmore et al.*, 2020b].

The late Oligocene/early Miocene age of the Rungwe Volcanic Province in southern Tanzania provides an upper estimate for the onset of EAR activity in northern Malawi [*Mesko*, 2020; *Mortimer et al.*, 2016b; *Rasskazov et al.*, 2001; *Roberts et al.*, 2012]. To the south, the onset of EAR extension is poorly constrained, with a Late Miocene-Pliocene age proposed for the central and southern basins of Lake Malawi from extrapolating modern depositional rates [*Delvaux*, 1995; *McCartney & Scholz*, 2016; *Scholz et al.*, 2020]. A southwards propagation of the EAR in Malawi is also consistent with the thinner sedimentary cover and smaller escarpment heights in southern Malawi [*Laõ-Dávila et al.*, 2015; *Wedmore et al.*, 2020a]. South of the Rungwe Volcanic Province, there has been no reported surface volcanism in the EAR, and only negligible amounts of melt are inferred in Malawi's lower crust and lithospheric mantle [*Accardo et al.*, 2017, 2020; *Hopper et al.*, 2020; *Njinju et al.*, 2019; *Wang et al.*, 2019].

In Malawi, the EAR can be divided along strike into several 50-200 km long basins that are each defined by one or more rift-bounding border faults, are commonly asymmetric, and are linked by high relief accommodation zones [Figure 2a; *Accardo et al.*, 2018; *Ebinger et al.*, 1987; *Laõ-Dávila et al.*, 2015; *McCartney & Scholz*, 2016; *Scholz*, 1989; *Scholz et al.*, 2020; *Wedmore et al.*, 2020b; *Williams et al.*, 2021]. Lake Malawi has flooded the three most northern EAR basins in Malawi [*Scholz et al.*, 2020], whilst to the south, the rift valley is onshore and channels the Shire River, Lake Malawi's only outlet, towards its confluence with the Zambezi River [*Dulanya*, 2017; *Ivory et al.*, 2016; *Williams et al.*, 2021].

In southern Malawi, active faults with surface traces were previously collated into the South Malawi Active Fault Database [SMAFD; *Williams et al.*, 2021]. However, elsewhere in Malawi, compilations of EAR faults depict faults at a coarser scale and with limited geomorphic or kinematic information [*Chapola & Kaphwiyo*, 1992; *Ebinger et al.*, 1987; *Macgregor*, 2015; *Styron & Pagani*, 2020]. In the written historical record (circa ~1870), only one active fault in Malawi has exhibited coseismic surface rupture, the St Mary Fault during the 2009 Karonga Earthquake sequence [*Biggs et al.*, 2010; *Gaherty et al.*, 2019; *Hamiel et al.*, 2012; *Kolawole et al.*, 2018b, 2018a; *Macheyeki et al.*, 2015].

3. The Malawi Active Fault Database (MAFD)

3.1 The MAFD fault mapping strategy

The Malawi Active Fault Database (MAFD) is a geospatial database of active fault traces. Seismic hazard planning is typically considered at the national level. Therefore, the MAFD is intended to cover all active faults within Malawi, and those close to its borders in Mozambique and Tanzania that may also contribute to seismic hazards. This definition closely follows the geological region of the 'Malawi Rift' or 'Nyasa Rift,' however, the Shire Rift Zone at the southern end of Malawi (Figure 2) is considered to represent a distinct part of the EAR [*Castaing*, 1991; *Kolawole et al.*, 2021]. Therefore, to avoid confusion we do not consider these geological regions further. Possible active faults within 20 km of Malawi in the Luangwa Rift in eastern Zambia [Figure 2; *Daly et al.*, 2020] are not included in the MAFD.

As with the SMAFD, faults in the MAFD are defined as active if they have accommodated displacement in the current (i.e., EAR) tectonic regime [*Williams et al.*, 2021]. Evidence for EAR activity on onshore faults includes steep linear scarps, offset sedimentary features such as alluvial fans, incised footwall drainage channels, and/or the accumulation of Post-Miocene sediment in the hanging-wall (Figure 3). All faults mapped under Lake Malawi are interpreted as active since all of them offset lake sediments, and so have been active during post-Miocene East African rifting.

Following the template used in the Global Earthquake Model Global Active Fault Database[GAF-DB; *Styron & Pagani*, 2020] faults in the MAFD, including those that show branching geometry, are mapped as a single continuous GIS feature. For each fault, a number of attributes are assigned that detail its geomorphic attributes and provide confidence that it is active (Table 1). Not all attributes (e.g., slip rates) included in the GAF-DB can be provided in the MAFD as these data are yet to be collected. Faults that influence topography, but do not meet the MAFD criteria for being active have been included in a separate database ('Malawi Other Faults,' Figure 2). Although these faults do not display evidence for recent activity, we cannot definitively exclude the possibility of reactivation.

3.2 Datasets for mapping faults in Malawi

3.2.1. High resolution digital elevation models

The primary source for mapping onshore active faults in the MAFD were TanDEM-X digital elevation models (DEMs) with a 12.5 m horizontal resolution and absolute vertical mean error of 0.2 m [*Wessel et al.*, 2018]. Previous analyses have demonstrated that scarps >5 m high can be clearly identified in TanDEM-X data for Malawi, and that the data can be used to measure along-strike scarp height variation [*Hodge et al.*, 2018a, 2019; *Wedmore et al.*, 2020b, 2020a]. The Mwanza and Nsanje faults extend into Mozambique and outside the region covered by the TanDEM-X data. These sections were instead mapped using the Shuttle Radar Topography Mission (SRTM) 30m resolution DEM [*Sandwell et al.*, 2011]. Active fault traces identified in the TanDEM-X data were verified in the field in south Malawi (Figure 3), and these traces were also compared against 1:100000 scale geological maps that were compiled across Malawi between the 1950s and 1970s [*Bloomfield*, 1958; *Bloomfield & Garson*, 1965; *Dawson & Kirkpatrick*, 1968; *Habgood*, 1963; *Habgood et al.*, 1973; *Harrison & Chapusa*, 1975; *Hopkins*, 1973; *Peters*, 1975; *Ray*, 1975; *Thatcher*, 1975]. Further details on the use of TanDEM-X data, fieldwork, and geological maps to identify active fault traces in Malawi are provided in *Hodge et al.*, [2018a; 2019], *Wedmore et al.*, [2020a; 2020b], and *Williams et al.*, [2021].

3.2.2. Seismic Reflection Data

Approximately 3500 km of 2D multichannel seismic reflection data across Lake Malawi were acquired between 1985-1987 through Project PROBE [Figure 4a; *Flannery & Rosendahl*, 1990; *Scholz & Rosendahl*, 1988; *Specht & Rosendahl*, 1989]. This survey extended over the entire lake with a 10-20 km line spacing and provided the first generation of maps detailing the structure and stratigraphy of Lake Malawi. Basin structure was subsequently revised in parts of the basin following collection of single-channel high-resolution data between 1992-1995 [*McCartney & Scholz*, 2016; *Mortimer et al.*, 2007; *Scholz*, 1995], and revised again following reprocessing of the Project PROBE data and its integration with 2000 km of 2D multichannel seismic reflection data from Lake Malawi's Central and North basins acquired through the Study of Extension and maGmatism in Malawi aNd Tanzania (SEGMeNT) project [Figure 4a; *Scholz et al.*, 2020; *Shillington et al.*, 2016, 2020]. The SeGMENT survey was acquired in an orthogonal grid with an average spacing of 8 km. In addition, the SeGMENT project deployed lake-bottom seismometers and collected wide angle seismic refraction data [*Accardo et al.*, 2018; *Shillington et al.*, 2020], which were used for assessments of the deeper crustal structure and depth migration of the seismic reflection data. Further details on data acquisition and processing are available in *Shillington et al.*, [2016, 2020], and *Scholz et al.*, [2020].

Faults within Lake Malawi are incorporated into the MAFD from offsets on the synrift basement surface, which was generated from an interpretation of all available seismic reflection data using a least-squares algorithm with a 750 x 750 m cell size [*Scholz et al.*, 2020]. Faults that offset this basement surface were mapped as 2D heave polygons (Figures 5 and 6); however, for inclusion in the MAFD, in which faults are mapped as 1D traces, only the footwall cutoffs of these heave polygons are utilized. Active faults in Lake Malawi could be alternatively mapped on a megadrought horizon, which is the near top of the sedimentary package and has been dated through drill-core to 75 ka [*Scholz et al.*, 2007; *Shillington et al.*, 2020]. However, by incorporating basement-rooted faults, we avoid the risk of omitting active faults that do not offset the near surface reflectors, and of including basement faults that splays in Lake Malawi's sedimentary package [*McCartney & Scholz*, 2016; *Mortimer et al.*, 2016a; *Scholz et al.*, 2020; *Shillington et al.*, 2020] as several distinct faults.

3.2.3. Aeromagnetic and Gravity data

Faults that are rooted into the magnetic crystalline basement, which may be surface-breaking or may be buried beneath sediments, can be mapped from aeromagnetic data. In aeromagnetic grids, faults are expressed as prominent linear magnetic gradients or as linear discontinuities that offset the lateral continuity of the basement fabrics [*Kolawole et al.*, 2018b, 2018a, 2021]. We utilize high resolution aeromagnetic data that were acquired in 2013 by the Geological Survey Department of Malawi at 250 m line spacing and 80 m flight altitude, and has a spatial resolution of ~62 m [*Dawson et al.*, 2018; *Kolawole et al.*, 2018a; *Laõ-Dávila et al.*, 2015]. Except for the Nsanje Basin (Figure 2a), the survey covers all onshore parts of

Malawi and extends up to 10 km offshore into Lake Malawi. Prior to fault interpretation, the total magnetic intensity aeromagnetic grid is first pole-reduced to correct for latitude-dependent skewness of the magnetic intensity data [*Arkani-Hamed*, 1988; *Baranov*, 1957]. Afterward, mathematical derivative filters are applied to the pole-reduced grids to better resolve magnetic gradients which reveal the basement structures. Faults are mapped along the edges of the abrupt linear gradients in the vertical derivative maps or along the 0°tilt-angle derivative contour of the tilt derivative maps, both of which are interpreted to represent the footwall cut-off for the top of basement fault offset [*Kolawole et al.*, 2018a].

Using the filtered aeromagnetic grids, *Kolawole et al.*, [2018b, 2018a] mapped faults buried beneath ~500 m of sediments in the Karonga region in northern Malawi, which we have subsequently incorporated into the MAFD (Figure 5). In southern Malawi, we consider faults previously mapped by *Kolawole et al.*, [2021] in two ways: (1) to identify faults with no surface expression (Figure 6), and (2) to revise the length of faults previously collated in the SMAFD in cases where the aeromagnetic signature of a fault extends beyond its surface expression [Figure 6; *Williams et al.*, 2021]. In the Lower Shire Valley, faults identified in gravity data are also included [*Chisenga et al.*, 2019].

Aeromagnetic and gravity data alone cannot be used to differentiate whether faults are active given the criteria in Section 3.1. We therefore only include faults identified in these data that strike between NW-SE and NNE-SSW, which means, assuming that they dip at a moderate angle, they are favorably oriented for normal fault reactivation under the region's ENE-WSW trending σ_3 [*Delvaux & Barth*, 2010;

Ebinger et al., 2019; *Williams et al.*, 2019]. We also omit faults that have a topographic expression (e.g., an escarpment, valley) which does not show evidence for EAR activity (Figure 6). In offshore areas, the extent of faults mapped in 2D seismic reflection surveys was extended where their trace could be correlated with the aeromagnetic data (Figures 5 and 6). NW-SE to NNE-SSW striking offshore faults identified in the aeromagnetic surveys but not in the seismic reflection surveys were also included in the MAFD, as we cannot exclude the possibility that these are active faults that have not yet propagated to the synrift basement. Faults identified in the aeromagnetic data that are not included in the MAFD are incorporated into the 'Malawi Other Faults' database (Figures 2b and 6).

3.3 Fault length distribution analysis

We use the distribution of fault lengths in the MAFD to test the hypothesis that their distribution will evolve from a power law to exponential trend as rift extension proceeds [*Ackermann et al.*, 2001; *Gupta & Scholz*, 2000; *Michas et al.*, 2015]. We first consider the length of each distinct continuous fault trace in the MAFD. Where faults splay in map view, only the length of the longest branch is considered, so that the full extent of fault lengthening is assessed. As the transition in fault length distribution is thought to arise from previously distinct faults linking, we also assess fault lengths under a 'multi-fault' scenario. In this case, we identify *en-echelon* faults that are currently mapped as distinct structures in the MAFD, but which may represent a single 'soft-linked' structure that could eventually coalesce into a 'hard-linked' faults as rift extension proceeds.

Empirical observations and Coulomb stress modelling indicate that two en-echelon normal faults may behave as a single soft-linked structure through co-seismic stress change transfer when the across-strike distance between the two fault tips is <20% of the participating faults' total length, up to a maximum across-strike distance of 10 km [*Biasi & Wesnousky*, 2016; *Hodge et al.*, 2018b]. We therefore use this as a criterion to determine if two en-echelon faults in Malawi may be part of a 'multi-fault' system.

We then test whether the distributions of fault and multi-fault lengths in the MAFD are best described by a power law or exponential distribution function through a two sample Kolmogorov Smirnov (KS) test [*Clauset et al.*, 2009; *Massey*, 1951]. We first use a Maximum Likelihood Estimator (MLE) to fit power law and exponential functions to the fault length data. This requires defining a lower bound of fault length (l_{min}), below which fault mapping is considered incomplete [*Clauset et al.*, 2009]. The complementary cumulative distribution function (cCDF, i.e., survival function), which is defined as the probability that the continuous variable L ≥ fault length (l), can then be expressed for a power law distribution as:

$$P_r(L \geq l) = \begin{cases} \left(\frac{l}{l_{min}}\right)^{1-\alpha}, & for\ l \geq l_{min}; \\ 1, & for\ l < l_{min} \end{cases} \quad (1)$$

where α is the power-law exponent. For an exponential distribution, the equivalent expression is:

$$P_r(L \geq l) = \begin{cases} e^{\lambda(l-l_{min})}, & for\ l \geq l_{min}; \\ 1, & for\ l < l_{min} \end{cases} \tag{2}$$

where λ is the rate parameter [*Clauset et al.*, 2009]. We then test the null hypothesis that the empirical cCDF function of fault lengths in the MAFD represents samples from these continuous theoretical functions. This is achieved by determining the maximum difference between the empirical and theoretical cumulative trends, *D**, and the probability (*p*) that *D** would have been observed given the null hypothesis and the number of available samples. In this analysis, the null hypothesis that the observed lengths are samples from a theoretical distribution is rejected if $p < 0.1$ [*Clauset et al.*, 2009].

To define l_{min}, we note that grid spacing of the 2D seismic surveys in Lake Malawi is 5-20 km (Figure 4) whilst TanDEM-X data can resolve scarps of 5 m in height [*Hodge et al.*, 2019; *Wedmore et al.*, 2020a] which corresponds to 1-10 km long faults given standard length-displacement scaling relationships [*Torabi & Berg*, 2011]. We therefore consider that l_{min} for the MAFD likely lies between 5-30 km and apply the two sample KS test at 1 km increments of l_{min} in this range. The magnitude of EAR extensional strain decreases from north to south in Malawi [*Scholz et al.*, 2020] whilst the techniques used to map onshore and offshore faults also varies. These factors have been observed to influence fault length distribution [*Michas et al.*, 2015]. We therefore repeat this analysis separately for faults mapped offshore in Lake Malawi and onshore in south Malawi.

As with investigations of all natural fault populations, this analysis has limitations, such as the relatively small range of fault lengths considered [typically 1-2 orders of magnitude; *Ackermann et al.*, 2001; *Clark et al.*, 1999; *Gupta & Scholz*, 2000]. and whether the mapped trace of a fault represents its true length [*Ackermann et al.*, 2001; *Clark et al.*, 1999]. This latter point is particularly important for offshore faults where uncertainties in fault lengths and potential linkages are constrained by the line spacing of 2D seismic reflection surveys [*Michas et al.*, 2015].

4. Results

4.1 Overview of the MAFD

The MAFD contains geospatial and geomorphic data on 114 active fault traces in Malawi and its surrounding regions (Figure 2, Table 1). Malawi's national borders broadly coincide with the trajectory of the EAR, and hence active faults are found along its length. There are, however, areas in western Malawi that may be up to 100 km from a mapped active fault (Figure 2). The MAFD, along with the 'Malawi Other Faults' database, is freely available for evaluating Malawi's seismic hazard or tectonic evolution (see Supplementary Information).

The MAFD has been compiled from a multidisciplinary range of datasets: 41 faults from high resolution DEMs [*Hodge et al.*, 2018a, 2019; *Wedmore et al.*, 2020a, 2020b; *Williams et al.*, 2021], 21 from aeromagnetic data [*Kolawole et al.*, 2018a, 2021], 4 from gravity data [*Chisenga et al.*, 2019], and 48 offshore faults in Lake Malawi from 2D seismic reflection surveys [*Scholz et al.*, 2020; *Shillington et al.*, 2020]. Further descriptions of these faults are provided in the referenced studies. The key innovations of the MAFD are that the faults identified in these datasets have been mapped in a uniform fashion, consistent criteria have been applied to classify fault activity (Section 3), and geomorphic and confidence attributes have been associated with each fault (Table 1). In south Malawi, the MAFD represents an update of the South Malawi Active Fault Database (SMAFD) as new fault mapping from aeromagnetic data [*Kolawole et al.*, 2021] has been used to: (1) revise the length of 9 faults that were in the SMAFD, and (2) identify 16 faults with no surface expression that were not included in the SMAFD (Figure 6b).

Under the 'activity_confidence' parameter (Table 1), high confidence could be placed for recent activity on faults mapped from seismic reflection surveys as they inherently offset EAR-age sediments. Faults that exhibit steep scarps in DEM's are also assigned high levels of confidence for recent activity, as scarps degrade relatively quickly in Malawi's subtropical climate [*Hodge et al.*, 2020]. The quality of mapping, in terms of accuracy and exposure quality (Table 1), was also high for these faults. Low levels of confidence are placed on recent activity along faults with degraded escarpments and buried faults identified in aeromagnetic and gravity data. The accuracy of fault mapping in seismic reflection data is relatively low as their position could only be constrained within the 5-20 km spaced 2D survey lines.

4.2 Onshore faults in Central Malawi

We highlight onshore faults in central Malawi as these faults are not typically considered in the region's tectonic evolution or seismic hazard. Evidence of recent activity on nine faults was identified in this region when compiling the MAFD. For example, the west-dipping Sani and Chilangali fault scarps impede streams flowing eastward into Lake Malawi, and in the case of the latter has resulted in the formation of Lake Chilangali [Figure 3b; *Harrison & Chapusa*, 1975]. Furthermore, the Liwaladzi scarp has diverted the Bua river [Figure 3b; *Harrison & Chapusa*, 1975;

Peters, 1975]. However, at its southern end, rivers have incised through the hanging wall of the Chilingali fault (Figure 3b).

4.3 Probability-distribution of fault lengths in the MAFD

Assuming that each fault in the MAFD represents a distinct structure, we can reject the null hypothesis that the distribution of their lengths is drawn from an exponential trend (i.e., $p<0.1$) for cases with a lower bound of fault length (l_{min}) >6 km (Figure 7b). However, we cannot reject the null hypothesis that the distribution of lengths may form a power law relationship with an exponent (α in equation 1) of 1.9 ± 0.2 when l_{min} > 10 km (Figures 7b-d and S1). With increasing l_{min}, α increases to 2.7 ± 0.5 (Figures 7b-d and S1).

Assuming the ‘multi-fault’ case, in which closely spaced en-echelon faults are considered to represent a single coherent structure, it is less clear which trend best describes the fault population (Figure 7e-f). When l_{min} <14 km, a power law hypothesis can be rejected, however, neither hypothesis can be rejected if l_{min} >14 km (Figure 7b). For the multi-fault power law trend, α is 1.8 ± 0.2 for l_{min} = 14 km, and 2.2 ± 0.4 for l_{min} = 30 km (Figure S1). For an exponential trend, the characteristic length-scale (1/λ, where λ is the rate parameter as defined in equation 2) ranges from 62 ± 18 km to 81 ± 30 km with increasing l_{min} (Figure S1).

We cannot reject the null hypothesis that fault lengths in Lake Malawi follow a power law distribution when l_{min} >11 km, and an exponential trend where the characteristic length-scale is 38 ± 15 km cannot be rejected when l_{min} <15 km (Figure S2). Neither hypothesis can be rejected for the multi-fault case when l_{min} >15 km for faults in Lake

Malawi (Figure S2e&f) or for any value of l_{min} in south Malawi (Figure S3). However, in these instances the distributions are drawn from a small number of faults (<50), and so caution should be applied when considering the significance of these results [*Clauset et al.*, 2009]. In summary, we do not consider that dividing faults in the MAFD between Lake Malawi and southern Malawi changes our initial interpretation that the distribution of fault lengths follows a power law trend for l_{min} >10 km, whilst neither hypothesis can be rejected for the multi-fault case.

5. Discussion

5.1 Completeness of the MAFD

The MAFD represents a compilation of all known fault traces in Malawi that show evidence for activity related to EAR extension. It does not, however, represent a database of every active fault in Malawi. Some active faults may be included in the 'Malawi Other Faults' databases (Figure 2) if they are active but there is currently no evidence for it. Furthermore, there are also likely hitherto unrecognised faults in Malawi that are not included in the MAFD. For example, up to 30% of the extension within Lake Malawi could be accommodated by faults that are below the resolution of seismic reflection data [*Marrett & Allmendinger*, 1992; *Shillington et al.*, 2020] or are not covered by the 5-20 km spaced seismic survey grid. Additionally, offshore faults with basement displacements less than ~100 ms were not mapped by *Scholz et al.*, [2020] as these were generally too short to correlate between multiple seismic profiles.

The MAFD includes faults that have no surface expression, but which can be identified in aeromagnetic data [*Kolawole et al.*, 2018a, 2021] and that have a favorable orientation for reactivation. This is an important step given that the 1989 Mw 6.3 Salima Earthquake, Malawi's largest instrumentally recorded earthquake, did not rupture to the surface [*Gupta*, 1992; *Jackson & Blenkinsop*, 1993]. The St Mary Fault also did not have a surface expression prior to rupturing in the 2009 Karonga earthquake sequence [*Kolawole et al.*, 2018a; *Macheyeki et al.*, 2015]. Nevertheless, since aeromagnetic grids are potential fields data that are typically unable to resolve deep basement-confined short-wavelength high-frequency anomalies, it is likely that deeply-buried small-offset faults were not identified [*Kolawole et al.*, 2017]. Faults that have not propagated to, and hence do not offset, the synrift basement surface, which lies 1-5 km under Lake Malawi [*Scholz et al.*, 2020], would also not be included in the MAFD.

Assuming that the power law distributions in Figure 7 are a true representation of fault lengths in Malawi, then these distributions imply that the MAFD is close to complete for fault lengths >10 km. However, caution should be applied to this interpretation given the heterogeneity of datasets. In either case, there are likely many active faults <10 km long that are not included in the MAFD.

Since we use evidence of displacement in the current EAR tectonic regime as a test for fault activity in the MAFD, and not a chronostratigraphic age (Section 3.1), it is possible that some currently inactive faults are included in this database. We also note that there is no unequivocal evidence that buried faults identified in aeromagnetic data have accommodated EAR extension. Nevertheless, recent activity on the majority of basement-rooted faults in Lake Malawi can be demonstrated by their offset of the 75 Ka megadrought horizon near the top of the lake's sedimentary package [*Scholz et al.*, 2007, 2020; *Shillington et al.*, 2020]. In addition, some of these faults show lake floor scarps [Figure 6e; *Crow & Eccles*, 1980; *Shillington et al.*, 2020]. More widely, assuming faults dip at ~40-65º, the generally NW-SE to NNE-SSW striking faults in the MAFD are favorably oriented for normal fault reactivation under the current ENE-WSW trending minimum principal compressive stress [Figure 8; *Ebinger et al.*, 2019; *Williams et al.*, 2019]. Depending on their position around neighboring faults, favorably oriented faults can still become inactive [*Cowie*, 1998]; however, this process mainly occurs at a stage when fault coalescence starts to dominate over fault nucleation [*Ackermann et al.*, 2001; *Hardacre & Cowie*, 2003], and the power-law distribution of fault lengths we document suggests this is not yet occurring in Malawi. Nevertheless, it is clear that further geophysical data should be collected and on-fault paleoseismic investigations undertaken to refine active fault mapping in Malawi.

5.2 The MAFD and seismic hazard in Malawi

The identification of active faults that are >50 km-long across the length of Malawi supports previous studies that suggest earthquakes M_W >7 may occur throughout the country [*Ebinger et al.*, 2019; *Hodge et al.*, 2015, 2020; *Jackson & Blenkinsop*, 1997; *Wedmore et al.*, 2020a; *Williams et al.*, 2021]. Therefore, regions of high seismic hazard in Malawi are not necessarily associated with those that have experienced recent earthquakes [*Hodge et al.*, 2015]. However, low regional extensional rates [0.5-2 mm/yr; *Stamps et al.*, 2018; *Wedmore et al.*, in review] imply large magnitude events would be rare [fault recurrence intervals ~1,000-20,000 years; *Hodge et al.*, 2015; *Shillington et al.*, 2020; *Williams et al.*, 2021].

Seismic hazard is most frequently considered in terms of ground shaking through Probabilistic Seismic Hazard Analysis. The MAFD can be used as a primary source for assessing this hazard, and also for the hazards associated with fault displacement [*Baize et al.*, 2019; *Hart & Bryant*, 1999; *Villamor et al.*, 2012] and liquefaction, which was observed after the 2009 Karonga earthquakes [*Kolawole et al.*, 2018b]. The presence of active faults adjacent to and below Lake Malawi may also warrant an investigation for the risk posed by earthquake triggered landslides, seiches, and tsunamis [*Moernaut et al.*, 2017; *Power et al.*, 2005; *Schnellmann et al.*, 2002].

The MAFD alone, however, cannot be used to assess these hazards, as no information is given on the magnitude or frequency of earthquakes that the documented faults may host. The data and analysis that is required for this information is often subjective and liable to change as data quality improves and epistemic uncertainties reduce. As such it is now common practice in seismic hazard assessment to distinguish clearly between the mapping of an active fault and its earthquake source properties [*Faure Walker et al.*, 2021; *Styron et al.*, 2020; *Williams et al.*, 2021]. A database that assesses the seismogenic properties of faults in Malawi will therefore be presented in future work.

5.3 Implications of the MAFD for understanding the tectonic evolution of the East African Rift in Malawi

A power law distribution of fault lengths is favoured in continental rifts when (1) fault growth occurs within a mechanically unconfined layer [*Ackermann et al.*, 2001; *Soliva & Schulz*, 2008] and/or, (2) total regional extension is low [<8-12% extension;

Gupta & Scholz, 2000; *Michas et al.*, 2015]. The power law distribution of fault lengths in the MAFD for l_{min} >10 km (Figure 7b), is therefore consistent with unconfined fault growth in Malawi's thick seismogenic crust [~35 km; *Craig & Jackson*, 2021; *Ebinger et al.*, 2019; *Jackson & Blenkinsop*, 1993] and low total extension in Malawi [< 8%; *Scholz et al.*, 2020].

The exponent (α~2) of the power distribution of fault lengths in Malawi is relatively high compared to other fault length distributions [α~1.5; *Clark et al.*, 1999; *Scholz & Cowie*, 1990]. This indicates a relatively high number of short faults in Malawi. It has been previously suggested that a power law distribution of fault lengths reflects localisation of regional strain onto a small number of relatively long faults [*Scholz & Cowie*, 1990; *Soliva & Schulz*, 2008]. This is broadly consistent with observations in Malawi that its longest faults (>100 km) tend to be hard-linked rift-bounding 'border' faults, which have accommodated 50-75% of rift extension [*Accardo et al.*, 2018; *Ebinger et al.*, 1987; *Shillington et al.*, 2020; *Wedmore et al.*, 2020b, 2020a].

Following the 'multi-fault' case to map faults in Malawi (Section 3.3), we identified 55 faults in the MAFD that may coalesce into 23 distinct structures, the majority of which are in intra-basinal domains. In this case, we cannot distinguish whether the length distribution follows an exponential or a power law distribution (Figure 7). Hence, although fault coalescence may facilitate the transition from a power law to an exponential distribution of fault lengths, it may not account for this transition alone. This suggests that as rift extension proceeds some shorter faults in Malawi may also need to become inactive for an exponential distribution of faults to form [*Hardacre & Cowie*, 2003; *Meyer et al.*, 2002].

6. Conclusions

We present the Malawi Active Fault Database (MAFD), a freely available geospatial database that contains geomorphic data on 114 active fault traces in Malawi. To address the challenges of mapping active faults in the Western Branch of the East African Rift's (EAR), the MAFD has been compiled from a multidisciplinary dataset that includes fieldwork, existing geological maps, high resolution digital elevation models [*Hodge et al.*, 2018a, 2019; *Wedmore et al.*, 2020a, 2020b; *Williams et al.*, 2021], seismic reflection data [*Scholz et al.*, 2020; *Shillington et al.*, 2016, 2020] aeromagnetic [*Kolawole et al.*, 2018a, 2021] and gravity data [*Chisenga et al.*, 2019]. We consider that the MAFD is currently the most complete active fault compilation across Malawi.

The MAFD documents active faults throughout Malawi. Previous analyses suggest that these faults are capable of M_W >7.0 earthquakes, however, the explicit analysis of these fault's seismic hazard is the focus of ongoing work. Nevertheless, exposure to seismic hazard in Malawi, and elsewhere in the EAR Western Branch is increasing due to rapid population growth and seismically vulnerable building stock. Similar datasets (e.g. seismic reflection and aeromagnetic data) to those used in the MAFD have already been collected elsewhere in the Western Branch [*Heilman et al.*, 2019; *Karp et al.*, 2012; *Katumwehe et al.*, 2015; *Kolawole et al.*, 2017, 2021; *McGlue et al.*, 2006; *Muirhead et al.*, 2019; *Wright et al.*, 2020]. We suggest that the MAFD framework for compiling and describing onshore and offshore active faults could be applied to these data for collecting primary fault observations to assess seismic hazard.

Through the MAFD we have also explored how active fault databases can be used to investigate regional geological evolution. We find that the distribution of fault lengths in the EAR in Malawi is not inconsistent with a power law. If true, this supports previous observations of strain localisation in Malawi along fully linked border fault systems, and studies elsewhere of low strain rifts in thick seismogenic crust [*Gupta & Scholz*, 2000; *Soliva & Schulz*, 2008]. As the EAR in Malawi accumulates more extension, we anticipate that shorter faults will coalesce together or become inactive to form an exponential distribution of fault lengths.

Acknowledgements and data availability

This work is supported by the EPSRC-Global Challenges Research Fund PREPARE (EP/P028233/1) and SAFER-PREPARED (part of the 'Innovative data services for aquaculture, seismic resilience and drought adaptation in East Africa' grant; EP/T015462/1) projects. TanDEM-X data were provided through DLR proposals DEM_GEOL0686 and DEM_GEOL2881. The Geological Survey Department of Malawi kindly gave us access to the 2013 aeromagnetic data across Malawi.

Seismic reflection data acquired through the Project PROBE and SEGMeNT Project are available through the Marine Geoscience Data System at: https://www.marine-geo.org/tools/search/entry.php?id=Malawi_PROBE (date last accessed at 05/25/21) and https://www.marine-geo.org/tools/entry/EARS_SEGMeNT (date last accessed 05/25/21) respectively. Aeromagnetic data for the Karonga region and southern Malawi are also archived on the Marine Geoscience Data System at: https://www.marine-geo.org/tools/search/Files.php?data_set_uid=24314 (DOI

doi:10.1594/IEDA/324314, date last accessed 05/25/21) and https://www.marine-geo.org/tools/search/Files.php?data_set_uid=24860 (DOI 10.1594/IEDA/324860, date last accessed 05/25/21) respectively. The Malawi Active Fault Database and Malawi Other Fault database are available as GIS shapefiles in the additional supplementary information to this article (Data Sets S1 and S2 respectively).

References

Accardo, N. J., Gaherty, J. B., Shillington, D. J., Ebinger, C. J., Nyblade, A. A., Mbogoni, G. J., et al. (2017). Surface wave imaging of the weakly extended Malawi Rift from ambient-noise and teleseismic Rayleigh waves from onshore and lake-bottom seismometers. *Geophysical Journal International*, *209*(3), 1892–1905. https://doi.org/10.1093/gji/ggx133

Accardo, N. J., Shillington, D. J., Gaherty, J. B., Scholz, C. A., Nyblade, A. A., Chindandali, P. R. N., et al. (2018). Constraints on Rift Basin Structure and Border Fault Growth in the Northern Malawi Rift From 3-D Seismic Refraction Imaging. *Journal of Geophysical Research: Solid Earth*, *123*(11), 10,003-10,025. https://doi.org/10.1029/2018JB016504

Accardo, N. J., Gaherty, J. B., Shillington, D. J., Hopper, E., Nyblade, A. A., Ebinger, C. J., et al. (2020). Thermochemical Modification of the Upper Mantle Beneath the Northern Malawi Rift Constrained From Shear Velocity Imaging. *Geochemistry, Geophysics, Geosystems*, *21*(6), 1–19. https://doi.org/10.1029/2019GC008843

Ackermann, R. V., Schlische, R. W., & Withjack, M. O. (2001). The geometric and statistical evolution of normal fault systems: An experimental study of the effects of mechanical layer thickness on scaling laws. *Journal of Structural Geology*, *23*(11), 1803–1819. https://doi.org/10.1016/S0191-8141(01)00028-1

Arkani-Hamed, J. (1988). Differential reduction-to-the-pole of regional magnetic anomalies. *Geophysics*, *53*(12), 1592–1600.

Avouac, J.-P. (1993). Analysis of scarp profiles: Evaluation of errors in morphologic dating. *Journal of Geophysical Research: Solid Earth*, *98*(B4), 6745–6754. https://doi.org/10.1029/92jb01962

Baize, S., Nurminen, F., Sarmiento, A., Dawson, T., Takao, M., Scotti, O., et al. (2019). A worldwide and unified database of surface ruptures (SURE) for fault displacement hazard analyses. *Seismological Research Letters*, *91*(1), 499–520. https://doi.org/10.1785/0220190144

Baranov, V. (1957). A new method for interpretation of aeromagnetic maps: pseudo-gravimetric anomalies. *Geophysics*, *22*(2), 359–382.

Bardet, J.-P., Synolakis, C. E., Davies, H. L., Imamura, F., & Okal, E. A. (2003). Landslide tsunamis: Recent findings and research directions. *Landslide Tsunamis: Recent Findings and Research Directions*, 1793–1809.

Biasi, G. P., & Wesnousky, S. G. (2016). Steps and gaps in ground ruptures: Empirical bounds on rupture propagation. *Bulletin of the Seismological Society of America*, *106*(3), 1110–1124. https://doi.org/10.1785/0120150175

Biggs, J., Nissen, E., Craig, T., Jackson, J., & Robinson, D. P. (2010). Breaking up the hanging wall of a rift-border fault: The 2009 Karonga earthquakes, Malawi. *Geophysical Research Letters*, *37*(11). https://doi.org/10.1029/2010GL043179

Bloomfield, K. (1958). The geology of the Port Herald Area. *Bulletin of the Geological Survey, Malawi*, *9*.

Bloomfield, K., & Garson, M. S. (1965). The Geology of the Kirk Range-Lisungwe Valley Area. *Bulletin of the Geological Survey, Malawi*, *17*.

Castaing, C. (1991). Post-Pan-African tectonic evolution of South Malawi in relation to the Karroo and recent East African rift systems. *Tectonophysics*, *191*(1–2), 55–73. https://doi.org/10.1016/0040-1951(91)90232-H

Chapola, L. S., & Kaphwiyo, C. E. (1992). The Malawi rift: Geology, tectonics and seismicity. *Tectonophysics*, *209*(1–4), 159–164. https://doi.org/10.1016/0040-1951(92)90017-Z

Chisenga, C., Dulanya, Z., & Jianguo, Y. (2019). The structural re-interpretation of the Lower Shire Basin in the Southern Malawi rift using gravity data. *Journal of African Earth Sciences*, *149*(September), 280–290. https://doi.org/10.1016/j.jafrearsci.2018.08.013

Clark, R. M., Cox, S. J. D., & Laslett, G. M. (1999). Generalizations of power-law distributions applicable to sampled fault-trace lengths: Model choice, parameter estimation and caveats. *Geophysical Journal International*, *136*(2), 357–372. https://doi.org/10.1046/j.1365-246X.1999.00728.x

Clauset, A., Shalizi, C. R., & Newman, M. E. J. (2009). Power-law distributions in empirical data. *SIAM Review*, *51*(4), 661–703. https://doi.org/10.1137/070710111

Cowie, P. A. (1998). A healing-reloading feedback control on the growth rate of seismogenic faults. *Journal of Structural Geology*, *20*(8), 1075–1087. https://doi.org/10.1016/S0191-8141(98)00034-0

Cowie, P. A., Sornette, D., & Vanneste, C. (1995). Multifractal scaling properties of a growing fault population. *Geophysical Journal International*, *122*(2), 457–469. https://doi.org/10.1111/j.1365-246X.1995.tb07007.x

Craig, T. J., & Jackson, J. A. (2021). Variations in the Seismogenic Thickness of East Africa. *Journal of Geophysical Research: Solid Earth*, *126*(3), 1–15. https://doi.org/10.1029/2020JB020754

Crow, M. J., & Eccles, D. H. (1980). A concealed active fault in the south-west arm of Lake Malawi. *Transactions, Geological Society of South Africa*, *83*(2), 297–299.

Daly, M. C., Green, P., Watts, A. B., Davies, O., Chibesakunda, F., & Walker, R. (2020). Tectonics and Landscape of the Central African Plateau and their Implications for a Propagating Southwestern Rift in Africa. *Geochemistry, Geophysics, Geosystems*, *21*(6). https://doi.org/10.1029/2019GC008746

Dawson, A. L., & Kirkpatrick, I. M. (1968). The geology of the Cape Maclear peninsula and Lower Bwanje valley. *Bulletin of the Geological Survey, Malawi*, *28*.

Dawson, S. M., Laó-Dávila, D. A., Atekwana, E. A., & Abdelsalam, M. G. (2018). The influence of the Precambrian Mughese Shear Zone structures on strain accommodation in the northern Malawi Rift. *Tectonophysics*, *722*, 53–68. https://doi.org/10.1016/j.tecto.2017.10.010

Delvaux, D. (1995). Age of Lake Malawi (Nyasa) and water level fluctuations. *Mus. Roy. Afrr. Centr., Tervuren (Belg.), Dept. Geol. Min., Rapp. Ann. 1993 & 1994*, *108*, 99–108.

Delvaux, D., & Barth, A. (2010). African stress pattern from formal inversion of focal mechanism data. *Tectonophysics*, *482*(1–4), 105–128. https://doi.org/10.1016/j.tecto.2009.05.009

Delvaux, D., Mulumba, J. L., Sebagenzi, M. N. S., Bondo, S. F., Kervyn, F., & Havenith, H. B. (2017). Seismic hazard assessment of the Kivu rift segment based on a new seismotectonic zonation model (western branch, East African

Rift system). *Journal of African Earth Sciences*, *134*, 831–855. https://doi.org/10.1016/j.jafrearsci.2016.10.004

Dulanya, Z. (2017). A review of the geomorphotectonic evolution of the south Malawi rift. *Journal of African Earth Sciences*. https://doi.org/10.1016/j.jafrearsci.2017.02.016

Ebinger, C. J., Rosendahl, B. R., & Reynolds, D. J. (1987). Tectonic model of the Malaŵi rift, Africa. *Tectonophysics*, *141*(1–3), 215–235. https://doi.org/10.1016/0040-1951(87)90187-9

Ebinger, C. J., Oliva, S. J., Pham, T. Q., Peterson, K., Chindandali, P., Illsley-Kemp, F., et al. (2019). Kinematics of Active Deformation in the Malawi Rift and Rungwe Volcanic Province, Africa. *Geochemistry, Geophysics, Geosystems*, *20*(8), 3928–3951. https://doi.org/10.1029/2019GC008354

Ekström, G., Nettles, M., & Dziewoński, A. M. (2012). The global CMT project 2004-2010: Centroid-moment tensors for 13,017 earthquakes. *Physics of the Earth and Planetary Interiors*, *200–201*, 1–9. https://doi.org/10.1016/j.pepi.2012.04.002

Evans, R. J., Ashwal, L. D., & Hamilton, M. A. (1999). Mafic, ultramafic, and anorthositic rocks of the Tete Complex, Mozambique: Petrology, age, and significance. *South African Journal of Geology*, *102*(2), 153–166.

Faure Walker, J., Paolo, B., Bruno, P., Gerald, R., & Lucilla, B. (2021). Fault2SHA Central Apennines database and structuring active fault data for seismic hazard assessment. *Scientific Data*, 1–20. https://doi.org/10.1038/s41597-021-00868-0

Field, E. H., Arrowsmith, R. J., Biasi, G. P., Bird, P., Dawson, T. E., Felzer, K. R., et al. (2014). Uniform California Earthquake Rupture Forecast, version 3 (UCERF3) -The time-independent model. *Bulletin of the Seismological Society*

of America, *104*(3), 1122–1180. https://doi.org/10.1785/0120130164
Flannery, J. W., & Rosendahl, B. R. (1990). The seismic stratigraphy of Lake Malawi, Africa: implications for interpreting geological processes in lacustrine rifts. *Journal of African Earth Sciences*, *10*(3), 519–548. https://doi.org/10.1016/0899-5362(90)90104-M
Foster, A. N., & Jackson, J. A. (1998). Source parameters of large African earthquakes: implications for crustal rheology and regional kinematics. *Geophysical Journal International*, *134*(2), 422–448. https://doi.org/10.1046/j.1365-246X.1998.00568.x
Fritz, H., Abdelsalam, M., Ali, K. A., Bingen, B., Collins, A. S., Fowler, A. R., et al. (2013). Orogen styles in the East African Orogen: A review of the Neoproterozoic to Cambrian tectonic evolution. *Journal of African Earth Sciences*. https://doi.org/10.1016/j.jafrearsci.2013.06.004
Fullgraf, T., Zammit, C., Bailly, L., Terrier, M., Hyvonen, E., Backman, B., et al. (2017). *Geological Mapping and Mineral Assessment Project (GEMMAP) of Malawi. Report Inception Phase - February 2017.*
Gaherty, J. B., Zheng, W., Shillington, D. J., Pritchard, M. E., Henderson, S. T., Chindandali, P. R. N., et al. (2019). Faulting processes during early-stage rifting: Seismic and geodetic analysis of the 2009-2010 Northern Malawi earthquake sequence. *Geophysical Journal International*, *217*(3), 1767–1782. https://doi.org/10.1093/gji/ggz119
Goda, K., Gibson, E. D., Smith, H. R., Biggs, J., & Hodge, M. (2016). Seismic risk assessment of urban and rural settlements around lake malawi. *Frontiers in Built Environment*, *2*. https://doi.org/10.3389/fbuil.2016.00030
Gràcia, E., Danobeitia, J., Vergés, J., Zitellini, N., Rovere, M., Accetella, D., et al.

(2003). Mapping active faults offshore Portugal (36°N-38°N): Implications for seismic hazard assessment along the southwest Iberian margin. *Geology*, *31*(1), 83–86. https://doi.org/10.1130/0091-7613(2003)031<0083:MAFOPN>2.0.CO;2

Gupta, A., & Scholz, C. H. (2000). Brittle strain regime transition in the Afar depression: Implications for fault growth and seafloor spreading. *Geology*, *28*(12), 1087–1090. https://doi.org/10.1130/0091-7613(2000)28<1087:BSRTIT>2.0.CO

Gupta, H. K. (1992). The Malawi earthquake of March 10, 1989: A report of the macroseismic survey. *Tectonophysics*, *209*(1–4), 165–166. https://doi.org/10.1016/0040-1951(92)90018-2

Habgood, F. (1963). The geology of the country west of the Shire River between Chikwawa and Chiromo. *Bulletin of the Geological Survey, Malawi*, *14*.

Habgood, F., Holt, D. N., & Walshaw, R. D. (1973). The geology of the Thyolo Area. *Bulletin of the Geological Survey, Malawi*, *22*.

Hamiel, Y., Baer, G., Kalindekafe, L., Dombola, K., & Chindandali, P. (2012). Seismic and aseismic slip evolution and deformation associated with the 2009-2010 northern Malawi earthquake swarm, East African Rift. *Geophysical Journal International*, *191*(3), 898–908. https://doi.org/10.1111/j.1365-246X.2012.05673.x

Hardacre, K. M., & Cowie, P. A. (2003). Controls on strain localization in a two-dimensional elastoplastic layer: Insights into size-frequency scaling of extensional fault populations. *Journal of Geophysical Research*, *108*(B11). https://doi.org/10.1029/2001jb001712

Harrison, D. R., & Chapusa, F. W. P. (1975). The geology of the Nkhotakota-Benga area. *Bulletin of the Geological Survey, Malawi*, *32*.

Hart, E., & Bryant, W. (1999). *Fault-rupture hazard zones in California: Alquist-Priolo Earthquake Fault Zoning Act with Index to Earthquake Fault Zones Maps*.

Heilman, E., Kolawole, F., Atekwana, E. A., & Mayle, M. (2019). Controls of Basement Fabric on the Linkage of Rift Segments. *Tectonics*, *38*(4), 1337–1366. https://doi.org/10.1029/2018TC005362

Hodge, M., Biggs, J., Goda, K., & Aspinall, W. (2015). Assessing infrequent large earthquakes using geomorphology and geodesy: the Malawi Rift. *Natural Hazards*, *76*(3), 1781–1806. https://doi.org/10.1007/s11069-014-1572-y

Hodge, M., Fagereng, A., Biggs, J., & Mdala, H. (2018a). Controls on Early-Rift Geometry: New Perspectives From the Bilila-Mtakataka Fault, Malawi. *Geophysical Research Letters*, *45*(9), 3896–3905. https://doi.org/10.1029/2018GL077343

Hodge, M., Fagereng, A., & Biggs, J. (2018b). The Role of Coseismic Coulomb Stress Changes in Shaping the Hard Link Between Normal Fault Segments. *Journal of Geophysical Research: Solid Earth*, *123*(1), 797–814. https://doi.org/10.1002/2017JB014927

Hodge, M., Biggs, J., Fagereng, A., Elliott, A., Mdala, H., & Mphepo, F. (2019). A semi-automated algorithm to quantify scarp morphology (SPARTA): Application to normal faults in southern Malawi. *Solid Earth*, *10*(1), 27–57. https://doi.org/10.5194/se-10-27-2019

Hodge, M., Biggs, J., Fagereng, Mdala, H., Wedmore, L. N. J., & Williams, J. N. (2020). Evidence From High-Resolution Topography for Multiple Earthquakes on High Slip-to-Length Fault Scarps: The Bilila-Mtakataka Fault, Malawi. *Tectonics*, *39*(2), e2019TC005933. https://doi.org/10.1029/2019TC005933

Hopkins, D. A. S. (1973). The geology of the Rumphi-Nkhata Bay area. *Bulletin of* *the Geological Survey, Malawi*, *38/39*.

Hopper, E., Gaherty, J. B., Shillington, D. J., Accardo, N. J., Nyblade, A. A., Holtzman, B. K., et al. (2020). Preferential localized thinning of lithospheric mantle in the melt-poor Malawi Rift. *Nature Geoscience*, *13*(8), 584–589. https://doi.org/10.1038/s41561-020-0609-y

Ivory, S. J., Blome, M. W., King, J. W., McGlue, M. M., Cole, J. E., & Cohen, A. S. (2016). Environmental change explains cichlid adaptive radiation at Lake Malawi over the past 1.2 million years. *Proceedings of the National Academy of Sciences of the United States of America*, *113*(42), 11895–11900. https://doi.org/10.1073/pnas.1611028113

Jackson, J., & Blenkinsop, T. (1993). The Malaŵi Earthquake of March 10, 1989: Deep faulting within the East African Rift System. *Tectonics*, *12*(5), 1131–1139. https://doi.org/10.1029/93TC01064

Jackson, J., & Blenkinsop, T. (1997). The Bilila-Mtakataka fault in Malawi: an active, 100-km long, normal fault segment in thick seismogenic crust. *Tectonics*, *16*(1), 137–150. https://doi.org/10.1029/96TC02494

Jackson, J., McKenzie, D., & Priestley, K. (2021). Relations between earthquake distributions, geological history, tectonics and rheology on the continents. *Philosophical Transactions of the Royal Society A: Mathematical, Physical and Engineering Sciences*, *379*(2193). https://doi.org/10.1098/rsta.2019.0412

Karp, T., Scholz, C. a., & McGlue, M. M. (2012). Structure and stratigraphy of the Lake Albert Rift, East Africa: observations from seismic reflections and gravity data. *Lacustrine Sandstone Reservoirs and Hydrocarbon Systems*, *99*, 299–318. https://doi.org/10.1306/13291394M952903

Katumwehe, A. B., Abdelsalam, M. G., & Atekwana, E. A. (2015). The role of preexisting Precambrian structures in rift evolution: The Albertine and Rhino grabens, Uganda. *Tectonophysics*, *646*, 117–129. https://doi.org/10.1016/j.tecto.2015.01.022

Kemp, J. (1975). The geology of the Uzumara area. *Bulletin of the Geological Survey, Malawi*.

Key, R. M., Bingen, B., Barton, E., Daudi, E. X. F., Manuel, S., & Moniz, A. (2007). Kimberlites in a Karoo graben of northern Mozambique: Tectonic setting, mineralogy and Rb-Sr geochronology. *South African Journal of Geology*, *110*(1), 111–124. https://doi.org/10.2113/gssajg.110.1.111

Kolawole, F., Atekwana, E. A., Malloy, S., Stamps, D. S., Grandin, R., Abdelsalam, M. G., et al. (2017). Aeromagnetic, gravity, and Differential Interferometric Synthetic Aperture Radar analyses reveal the causative fault of the 3 April 2017 Mw 6.5 Moiyabana, Botswana, earthquake. *Geophysical Research Letters*, *44*(17), 8837–8846. https://doi.org/10.1002/2017GL074620

Kolawole, F., Atekwana, E. A., Laó-Dávila, D. A., Abdelsalam, M. G., Chindandali, P. R., Salima, J., & Kalindekafe, L. (2018a). Active Deformation of Malawi Rift's North Basin Hinge Zone Modulated by Reactivation of Preexisting Precambrian Shear Zone Fabric. *Tectonics*, *37*(3), 683–704. https://doi.org/10.1002/2017TC004628

Kolawole, F., Atekwana, E. A., Laó-Dávila, D. A., Abdelsalam, M. G., Chindandali, P. R., Salima, J., & Kalindekafe, L. (2018b). High-resolution electrical resistivity and aeromagnetic imaging reveal the causative fault of the 2009 Mw 6.0 Karonga, Malawi earthquake. *Geophysical Journal International*, *213*(2), 1412–1425. https://doi.org/10.1093/gji/ggy066

Kolawole, F., Firkins, M. C., Al Wahaibi, T. S., Atekwana, E. A., & Soreghan, M. J.

(2021). Rift Transfer Zones and the Stages of Rift Linkage in Active Segmented Continental Rift Systems.

Langridge, R. M., Ries, W. F., Litchfield, N. J., Villamor, P., Van Dissen, R. J., Barrell, D. J. A., et al. (2016). The New Zealand Active Faults Database. *New Zealand Journal of Geology and Geophysics*, *59*(1), 86–96. https://doi.org/10.1080/00288306.2015.1112818

Laõ-Dávila, D. A., Al-Salmi, H. S., Abdelsalam, M. G., & Atekwana, E. A. (2015). Hierarchical segmentation of the Malawi Rift: The influence of inherited lithospheric heterogeneity and kinematics in the evolution of continental rifts. *Tectonics*, *34*(12), 2399–2417. https://doi.org/10.1002/2015TC003953

Lavayssière, A., Drooff, C., Ebinger, C., Gallacher, R., Illsley-Kemp, F., Oliva, S. J., & Keir, D. (2019). Depth Extent and Kinematics of Faulting in the Southern Tanganyika Rift, Africa. *Tectonics*, *38*(3), 842–862. https://doi.org/10.1029/2018TC005379

Lenoir, J. L., Liégeois, J. P., Theunissen, K., & Klerkx, J. (1994). The Palaeoproterozoic Ubendian shear belt in Tanzania: geochronology and structure. *Journal of African Earth Sciences*, *19*(3), 169–184. https://doi.org/10.1016/0899-5362(94)90059-0

Macgregor, D. (2015). History of the development of the East African Rift System: A series of interpreted maps through time. *Journal of African Earth Sciences*. https://doi.org/10.1016/j.jafrearsci.2014.09.016

Macheyeki, A. S., Mdala, H., Chapola, L. S., Manhiça, V. J., Chisambi, J., Feitio, P., et al. (2015). Active fault mapping in Karonga-Malawi after the December 19, 2009 Ms 6.2 seismic event. *Journal of African Earth Sciences*, *102*, 233–246. https://doi.org/10.1016/j.jafrearsci.2014.10.010

Manda, B. W. C., Cawood, P. A., Spencer, C. J., Prave, T., Robinson, R., & Roberts, N. M. W. (2019). Evolution of the Mozambique Belt in Malawi constrained by granitoid U-Pb, Sm-Nd and Lu-Hf isotopic data. *Gondwana Research*, *68*, 93–107. https://doi.org/10.1016/j.gr.2018.11.004

Marlow, M. S., Gardner, J. V., & Normark, W. R. (2000). Using high-resolution multibeam bathymetry to identity seafloor surface rupture along the Palos Verdes fault complex in offshore Southern California. *Geology*, *28*(7), 587–590. https://doi.org/10.1130/0091-7613(2000)28<587:UHMBTI>2.0.CO;2

Marrett, R., & Allmendinger, R. W. (1992). Amount of extension on “small’’ faults: an example from the Viking graben.” *Geology*, *20*(1), 47–50. https://doi.org/10.1130/0091-7613(1992)020<0047:AOEOSF>2.3.CO;2

Massey, F. J. (1951). The Kolmogorov-Smirnov Test for Goodness of Fit. *Journal of the American Statistical Association*, *46*(253), 68. https://doi.org/10.2307/2280095

Masson, D. G., Harbitz, C. B., Wynn, R. B., Pedersen, G., & Løvholt, F. (2006). Submarine landslides: Processes, triggers and hazard prediction. *Philosophical Transactions of the Royal Society A: Mathematical, Physical and Engineering Sciences*, *364*(1845), 2009–2039. https://doi.org/10.1098/rsta.2006.1810

McCartney, T., & Scholz, C. A. (2016). A 1.3 million year record of synchronous faulting in the hangingwall and border fault of a half-graben in the Malawi (Nyasa) Rift. *Journal of Structural Geology*, *91*, 114–129. https://doi.org/10.1016/j.jsg.2016.08.012

McGlue, M. M., Scholz, C. a., Karp, T., Ongodia, B., & Lezzar, K. E. (2006). Facies Architecture of Flexural Margin Lowstand Delta Deposits in Lake Edward, East African Rift. *Journal of Sedimentary Research*, *76*, 942–958.

https://doi.org/10.2110/jsr.2006.068

Mesko, G. (2020). Magmatism at the Southern End of the East African Rift System: Origin and Role During Early Stage Rifting. Columbia University.

Meyer, V., Nicol, A., Childs, C., Walsh, J. J., & Watterson, J. (2002). Progressive localisation of strain during the evolution of a normal fault population. *Journal of Structural Geology*, *24*(8), 1215–1231. https://doi.org/10.1016/S0191-8141(01)00104-3

Michas, G., Vallianatos, F., & Sammonds, P. (2015). Statistical mechanics and scaling of fault populations with increasing strain in the Corinth Rift. *Earth and Planetary Science Letters*, *431*, 150–163. https://doi.org/10.1016/j.epsl.2015.09.014

Midzi, V., Hlatywayo, D. J., Chapola, L. S., Kebede, F., Atakan, K., Lombe, D. K., et al. (1999). Seismic hazard assessment in Eastern and Southern Africa. *Annali Di Geofisica*. https://doi.org/10.4401/ag-3770

Moernaut, J., Van Daele, M., Strasser, M., Clare, M. A., Heirman, K., Viel, M., et al. (2017). Lacustrine turbidites produced by surficial slope sediment remobilization: a mechanism for continuous and sensitive turbidite paleoseismic records. *Marine Geology*, *384*, 159–176.

Mortimer, E. J., Paton, D. A., Scholz, C. A., Strecker, M. R., & Blisniuk, P. (2007). Orthogonal to oblique rifting: Effect of rift basin orientation in the evolution of the North basin, Malawi Rift, East Africa. *Basin Research*, *19*(3), 393–407. https://doi.org/10.1111/j.1365-2117.2007.00332.x

Mortimer, E. J., Paton, D. A., Scholz, C. A., & Strecker, M. R. (2016a). Implications of structural inheritance in oblique rift zones for basin compartmentalization: Nkhata Basin, Malawi Rift (EARS). *Marine and Petroleum Geology*, *72*, 110–

121. https://doi.org/10.1016/j.marpetgeo.2015.12.018
Mortimer, E. J., Kirstein, L. A., Stuart, F. M., & Strecker, M. R. (2016b). Spatio-temporal trends in normal-fault segmentation recorded by low-temperature thermochronology: Livingstone fault scarp, Malawi Rift, East African Rift System. *Earth and Planetary Science Letters*, *455*, 62–72. https://doi.org/10.1016/j.epsl.2016.08.040
Muirhead, J. D., Wright, L. J. M., & Scholz, C. A. (2019). Rift evolution in regions of low magma input in East Africa. *Earth and Planetary Science Letters*, *506*, 332–346. https://doi.org/10.1016/j.epsl.2018.11.004
Nicol, A., Van Dissen, R. J., Stirling, M. W., & Gerstenberger, M. C. (2016). Completeness of the Paleoseismic Active-Fault Record in New Zealand. *Seismological Research Letters*, *87*(6), 1299–1310. https://doi.org/10.1785/0220160088
Njinju, E. A., Kolawole, F., Atekwana, E. A., Stamps, D. S., Atekwana, E. A., Abdelsalam, M. G., & Mickus, K. L. (2019). Terrestrial heat flow in the Malawi Rifted Zone, East Africa: Implications for tectono-thermal inheritance in continental rift basins. *Journal of Volcanology and Geothermal Research*, *387*. https://doi.org/10.1016/j.jvolgeores.2019.07.023
Novelli, V., Kloukinas, P., De Risi, R., Kafodya, I., Ngoma, I., Macdonald, J., & Goda, K. (2019). Seismic Mitigation Framework for Non-engineered Masonry Buildings in Developing Countries: Application to Malawi in the East African Rift. In *Resilient Structures and Infrastructure* (pp. 195–223). Springer.
Nyblade, A. A., & Langston, C. A. (1995). East African earthquakes below 20 km depth and their implications for crustal structure. *Geophysical Journal International*, *121*(1), 49–62. https://doi.org/10.1111/j.1365-

246X.1995.tb03510.x

Peters, E. R. (1975). The geology of the south Viphya area. *Bulletin of the Geological Society of America*, *36*.

Poggi, V., Durrheim, R., Tuluka, G. M., Weatherill, G., Gee, R., Pagani, M., et al. (2017). Assessing seismic hazard of the East African Rift: a pilot study from GEM and AfricaArray. *Bulletin of Earthquake Engineering*, pp. 4499–4529. https://doi.org/10.1007/s10518-017-0152-4

Pondard, N., & Barnes, P. M. (2010). Structure and paleoearthquake records of active submarine faults, Cook Strait, New Zealand: Implications for fault interactions, stress loading, and seismic hazard. *Journal of Geophysical Research: Solid Earth*, *115*(12). https://doi.org/10.1029/2010JB007781

Power, W., Downes, G., McSaveney, M., Beavan, J., & Hancox, G. (2005). The Fiordland earthquake and tsunami, New Zealand, 21 August 2003. In *Tsunamis* (pp. 31–42). Springer.

Rasskazov, S. V, Logachev, N. A., Ivanov, A. V, Boven, A. A., Maslovskaya, M. N., Saranina, E. V, et al. (2001). The 19-17 ma magmatic episode in the Western rift of East Africa and its bearing on geodynamics. *Doklady Akademii Nauk-Rossijskaya Akademiya Nauk*, *381*(2), 230–233.

Ray, G. E. (1975). The geology of the Chitipa-Karonga area. *Bulletin of the Geological Survey, Malawi*, *42*.

Ring, U. (1993). Aspects of the kinematic history and mechanisms of superposition of the proterozoic mobile belts of eastern Central Africa (northern Malawi and southern Tanzania). *Precambrian Research*, *62*(3), 207–226. https://doi.org/10.1016/0301-9268(93)90022-T

Ring, U. (1994). The influence of preexisting structure on the evolution of the

Cenozoic Malawi rift (East African rift system). *Tectonics*, *13*(2), 313–326. https://doi.org/10.1029/93TC03188

Roberts, E. M., Stevens, N. J., O'Connor, P. M., Dirks, P. H. G. M., Gottfried, M. D., Clyde, W. C., et al. (2012). Initiation of the western branch of the East African Rift coeval with the eastern branch. *Nature Geoscience*, *5*(4), 289–294. https://doi.org/10.1038/ngeo1432

Sandwell, D., Mellors, R., Tong, X., Wei, M., & Wessel, P. (2011). Open radar interferometry software for mapping surface Deformation. *Eos, Transactions American Geophysical Union*. https://doi.org/10.1029/2011EO280002

Saria, E., Calais, E., Stamps, D. S., Delvaux, D., & Hartnady, C. J. H. (2014). Present-day kinematics of the East African Rift. *Journal of Geophysical Research: Solid Earth*, *119*(4), 3584–3600. https://doi.org/10.1002/2013JB010901

Schnellmann, M., Anselmetti, F. S., Giardini, D., McKenzie, J. A., & Ward, S. N. (2002). Prehistoric earthquake history revealed by lacustrine slump deposits. *Geology*, *30*(12), 1131–1134.

Scholz, C. A. (1989). *Seismic Atlas of Lake Malawi (Nyasa), East Africa*. Project PROBE, Duke University.

Scholz, C. A. (1995). Deltas of the Lake Malawi Rift, East Africa: seismic expression and exploration implications. *American Association of Petroleum Geologists Bulletin*, *79*(11), 1679–1697. https://doi.org/10.1306/7834de54-1721-11d7-8645000102c1865d

Scholz, C. A., & Rosendahl, B. R. (1988). Low lake stands in lakes Malawi and tanganyika, East Africa, delineated with multifold seismic data. *Science*, *240*, 1645–1648. https://doi.org/10.1126/science.240.4859.1645

Scholz, C. A., Johnson, T. C., Cohen, A. S., King, J. W., Peck, J. A., Overpeck, J. T., et al. (2007). East African megadroughts between 135 and 75 thousand years ago and bearing on early-modern human origins. *Proceedings of the National Academy of Sciences of the United States of America*, *104*(42), 16416–16421. https://doi.org/10.1073/pnas.0703874104

Scholz, C. A., Shillington, D. J., Wright, L. J. M., Accardo, N., Gaherty, J. B., & Chindandali, P. (2020). Intrarift fault fabric, segmentation, and basin evolution of the Lake Malawi (Nyasa) Rift, East Africa. *Geosphere*, *16*(5), 1293–1311. https://doi.org/10.1130/GES02228.1

Scholz, C. H., & Cowie, P. A. (1990). Determination of total strain from faulting using slip measurements. *Nature*, *346*(6287), 837–839. https://doi.org/10.1038/346837a0

Shillington, D. J., Gaherty, J. B., Ebinger, C. J., Scholz, C. A., Selway, K., Nyblade, A. A., et al. (2016). Acquisition of a unique onshore/offshore geophysical and geochemical dataset in the northern Malawi (Nyasa) rift. *Seismological Research Letters*, *87*(6), 1406–1416. https://doi.org/10.1785/0220160112

Shillington, D. J., Scholz, C. A., Chindandali, P. R. N., Gaherty, J. B., Accardo, N. J., Onyango, E., et al. (2020). Controls on Rift Faulting in the North Basin of the Malawi (Nyasa) Rift, East Africa. *Tectonics*, *39*(3), e2019TC005633. https://doi.org/10.1029/2019TC005633

Soliva, R., & Schulz, R. A. (2008). Distributed and localized faulting in extensional settings: Insight from the north Ethiopian Rift-Afar transition area. *Tectonics*, *27*(2). https://doi.org/10.1029/2007TC002148

Specht, T. D., & Rosendahl, B. R. (1989). Architecture of the Lake Malawi Rift, East Africa. *Journal of African Earth Sciences*, *8*(2–4), 355–382.

https://doi.org/10.1016/S0899-5362(89)80032-6

Stamps, D. S., Saria, E., & Kreemer, C. (2018). A Geodetic Strain Rate Model for the East African Rift System. *Scientific Reports*, *8*(1). https://doi.org/10.1038/s41598-017-19097-w

Stamps, D. S., Kreemer, C., Fernandes, R., Rajaonarison, T. A., & Rambolamanana, G. (2020). Redefining East African Rift System kinematics. *Geology*. https://doi.org/10.1130/g47985.1

Styron, R., & Pagani, M. (2020). The GEM Global Active Faults Database. *Earthquake Spectra*, *36*(1_suppl), 160–180. https://doi.org/10.1177/8755293020944182

Styron, R., García-Pelaez, J., & Pagani, M. (2020). CCAF-DB: The Caribbean and Central American active fault database. *Natural Hazards and Earth System Sciences*, *20*(3), 831–857. https://doi.org/10.5194/nhess-20-831-2020

Thatcher, E. C. (1975). The geology of the Nyika Region. *Bulletin of the Geological Survey, Malawi*, *40*.

Torabi, A., & Berg, S. S. (2011). Scaling of fault attributes: A review. *Marine and Petroleum Geology*. https://doi.org/10.1016/j.marpetgeo.2011.04.003

Versfelt, J., & Rosendahl, B. R. (1989). Relationships between pre-rift structure and rift architecture in Lakes Tanganyika and Malawi, East Africa. *Nature*, *337*(6205), 354–357. https://doi.org/10.1038/337354a0

Villamor, P., Litchfield, N., Barrell, D., Van Dissen, R., Hornblow, S., Quigley, M., et al. (2012). Map of the 2010 Greendale Fault surface rupture, Canterbury, New Zealand: Application to land use planning. *New Zealand Journal of Geology and Geophysics*, *55*(3), 223–230. https://doi.org/10.1080/00288306.2012.680473

Vittori, E., Delvaux, D., & Kervyn, F. (1997). Kanda fault: A major seismogenic element west of the Rukwa Rift (Tanzania, East Africa). *Journal of Geodynamics*, *24*(1–4), 139–153. https://doi.org/10.1016/S0264-3707(96)00038-5

Wallace, R. W. (1980). Degradation of the Hebgen Lake fault scarps of 1959. *Geology*, *8*(5), 225–229. https://doi.org/10.1130/0091-7613(1980)8<225:DOTHLF>2.0.CO;2

Walsh, J. J., Childs, C., Imber, J., Manzocchi, T., Watterson, J., & Nell, P. A. R. (2002). Strain localisation and population changes during fault system growth within the Inner Moray Firth, northern North Sea. *Journal of Structural Geology*, *25*(2), 307–315. https://doi.org/10.1016/S0191-8141(02)00028-7

Walshaw, R. D. (1965). The Geology of the Nchue-Balaka Area. *Bulletin of the Geological Survey, Malawi*, *19*.

Wang, T., Feng, J., Liu, K. H., & Gao, S. S. (2019). Crustal structure beneath the Malawi and Luangwa Rift Zones and adjacent areas from ambient noise tomography. *Gondwana Research*, *67*, 187–198. https://doi.org/10.1016/j.gr.2018.10.018

Wedmore, L. N. J., Biggs, J., Williams, J. N., Fagereng, Dulanya, Z., Mphepo, F., & Mdala, H. (2020a). Active Fault Scarps in Southern Malawi and Their Implications for the Distribution of Strain in Incipient Continental Rifts. *Tectonics*, *39*(3), e2019TC005834. https://doi.org/10.1029/2019TC005834

Wedmore, L. N. J., Williams, J. N., Biggs, J., Fagereng, Å., Mphepo, F., Dulanya, Z., et al. (2020b). Structural inheritance and border fault reactivation during active early-stage rifting along the Thyolo fault, Malawi. *Journal of Structural Geology*, *139*, 104097. https://doi.org/10.1016/j.jsg.2020.104097

Wedmore, L. N. J., Biggs, J., Floyd, M., Fagereng, Å., Mdala, H., Chindandali, P. R.

N., et al. (in review). Geodetic constraints on cratonic microplates and broad strain during rifting of thick Southern Africa lithosphere. *Geophysical Research Letters*.

Wessel, B., Huber, M., Wohlfart, C., Marschalk, U., Kosmann, D., & Roth, A. (2018). Accuracy assessment of the global TanDEM-X Digital Elevation Model with GPS data. *ISPRS Journal of Photogrammetry and Remote Sensing*, *139*, 171–182.

Williams, J. N., Fagereng, Å., Wedmore, L. N. J., Biggs, J., Mphepo, F., Dulanya, Z., et al. (2019). How Do Variably Striking Faults Reactivate During Rifting? Insights From Southern Malawi. *Geochemistry, Geophysics, Geosystems*, *20*(7), 3588–3607. https://doi.org/10.1029/2019GC008219

Williams, J. N., Mdala, H., Fagereng, Å., Wedmore, L. N. J., Biggs, J., Dulany, Z., et al. (2021). A systems-based approach to parameterise seismic hazard in regions with little historical or instrumental seismicity: Active fault and seismogenic source databases for southern Malawi. *Solid Earth*, *12*(1), 187–217. https://doi.org/10.5194/se-12-187-2021

Wopfner, H. (2002). Tectonic and climatic events controlling deposition in Tanzanian Karoo basins. *Journal of African Earth Sciences*, *34*(3–4), 167–177. https://doi.org/10.1016/S0899-5362(02)00016-7

Wright, L. J. M., Muirhead, J. D., & Scholz, C. A. (2020). Spatiotemporal Variations in Upper Crustal Extension Across the Different Basement Terranes of the Lake Tanganyika Rift, East Africa. *Tectonics*, *39*(3). https://doi.org/10.1029/2019TC006019

List of Tables

Table 1

Attribute	Type	Description	Notes
MAFD-ID	Numeric, assigned	Unique two-digit numerical reference ID for each trace	
fault_name	Text		Assigned based on previous mapping or local geographic feature.
dip_dir	Text	Compass quadrant that fault dips in.	
Geomorphic Expression	Text	Geomorphological feature used to identify and map fault trace.	E.g., scarp, escarpment
Location Method	Text	Dataset used to map trace.	E.g., type of digital elevation model
Accuracy	Numeric, assigned	Coarsest scale at which trace can be mapped. Expressed as denominator of map scale.	Reflects the prominence of the fault’s geomorphic expression.
activity_confidence	Numeric, assigned	Certainty of neotectonic activity	1 if certain, 2 if uncertain
exposure_quality	Numeric, assigned	Fault exposure quality	1 if high, 2 if low
epistemic_quality	Numeric, assigned	Certainty that fault exists there	1 if high, 2 if low

last_movement	Text		Currently this is unknown for all faults in Malawi except the St Mary' Fault.
notes	Text	Remaining miscellaneous information about fault.	
references	Text	Relevant geological maps/literature where fault has been previously described.	

Table 1: List and brief description of attributes in the MAFD. Attributes are based on the Global Earthquake Model Global Active Faults Database (Styron and Pagani, 2020).

List of Figures

Figure 1

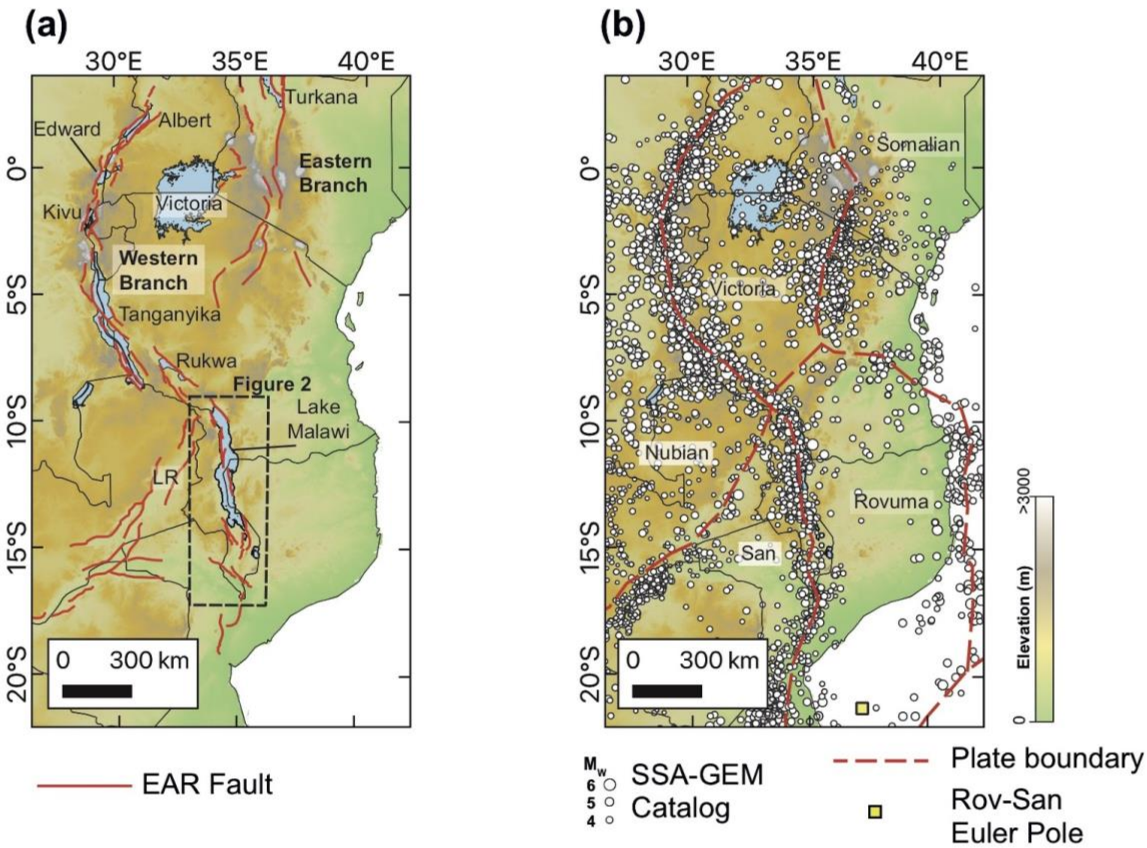

Figure 1: (a) The African Great Lakes in the context of the Western and Eastern branches of the East African Rift (EAR). Traces of major EAR faults compiled from the Global Earthquake Model Global Active Fault Database [*Styron & Pagani*, 2020], *Hodge et al.*, [2018a] and *Daly et al.*, [2020]. LR; Luangwa Rift. Equivalent to (b) but showing the EAR microplate boundaries, Rovuma-San Euler Pole [*Wedmore et al.*, in review], and earthquake locations from the Sub-Saharan Africa Global Earthquake Model Catalog [SSA-GEM; *Poggi et al.*, 2017]. Images underlain by Global 30 Arc-Second Elevation (GTOPO30) Digital Elevation Model.

Figure 2

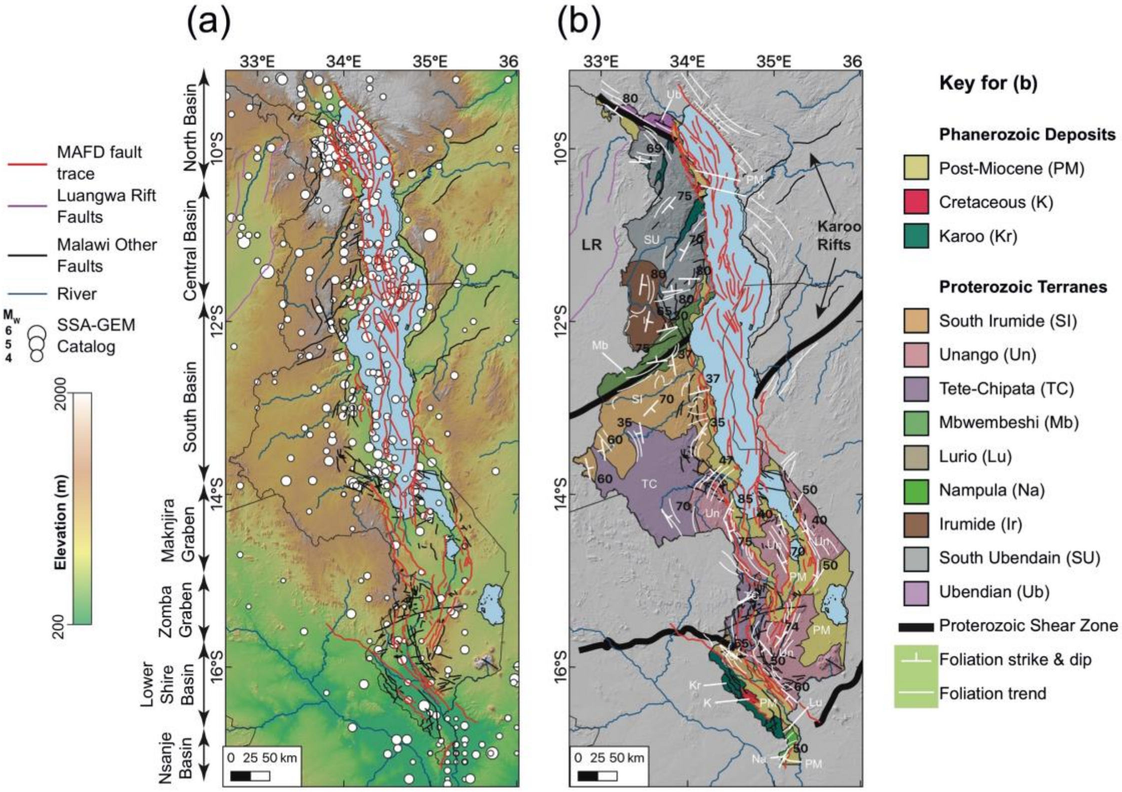

Figure 2: The Malawi Active Fault Database (MAFD) in the context of (a) a Shuttle Radar Topography Mission (SRTM) 30 m digital elevation model (DEM) and (b) simplified geological map of Malawi [*Fullgraf et al.*, 2017]. In (a) previously defined EAR rift segments in Malawi are shown along the western edge of the map [*Scholz et al.*, 2020; *Williams et al.*, 2021]. SSA-GEM; Sub-Saharan African Global Earthquake Model catalog [*Poggi et al.*, 2017]. Foliation measurements in (b) are compiled from legacy geological maps [*Bloomfield*, 1958; *Bloomfield & Garson*, 1965; *Dawson & Kirkpatrick*, 1968; *Habgood*, 1963; *Habgood et al.*, 1973; *Harrison & Chapusa*, 1975; *Hopkins*, 1973; *Peters*, 1975; *Ray*, 1975; *Thatcher*, 1975], and shown with major Proterozoic shear zones [*Evans et al.*, 1999; *Laõ-Dávila et al.*, 2015], and dominant foliation trends as mapped from geological maps, aeromagnetic data, and SRTM 30 m DEM.

Figure 3

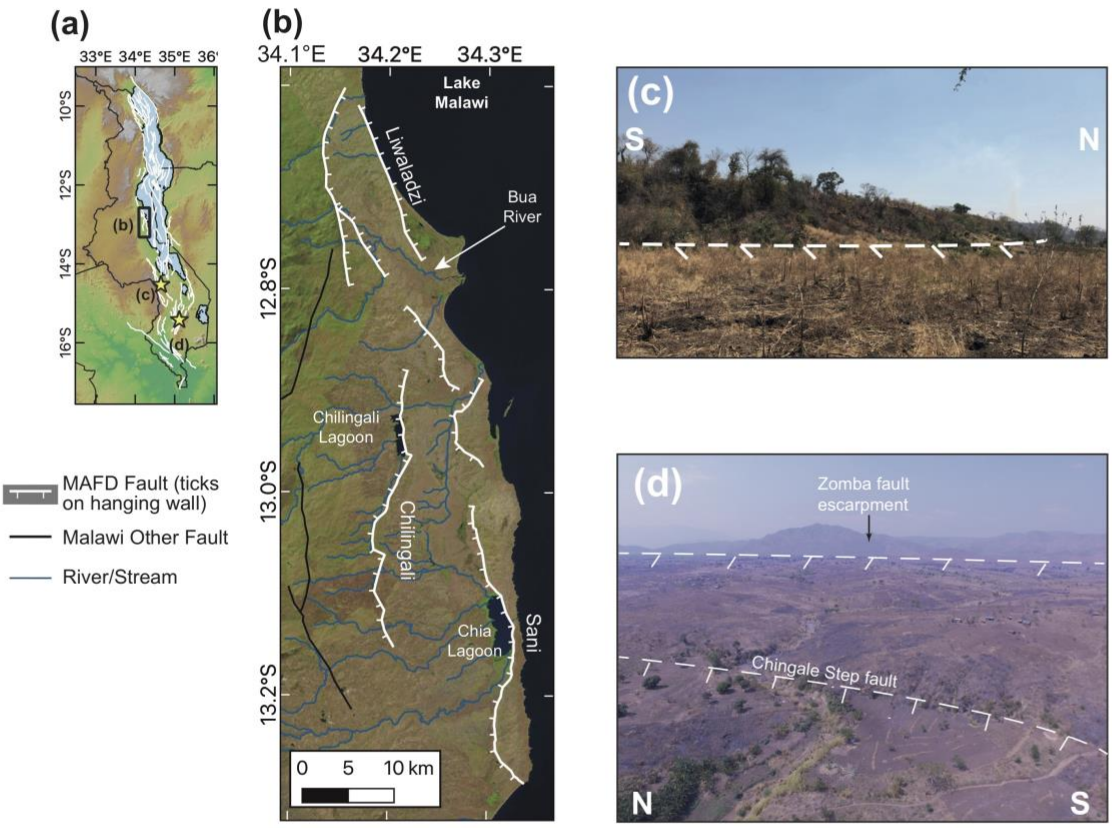

Figure 3: Examples of onshore faults in the MAFD with a surface expression. Figure locations given in (a), where white lines show the MAFD fault traces. (b) Landsat 8 natural colour image underlain by Shuttle Radar Topography Mission (SRTM) 30 m digital elevation model showing interactions between active onshore faults and rivers and streams in central Malawi. Note, Chia Lagoon has not formed from the impediment of streams flowing into the Sani fault footwall, and instead water flows from Lake Malawi into the lagoon via an artificial cut. (c) Soil-mantled scarp of the Kasinje section of the Bilila-Mtakataka fault [*Hodge et al.*, 2020]. (d) Unmanned Aerial Vehicle (UAV) image of the Chingale Step fault scarp with the Zomba fault escarpment behind.

Figure 4

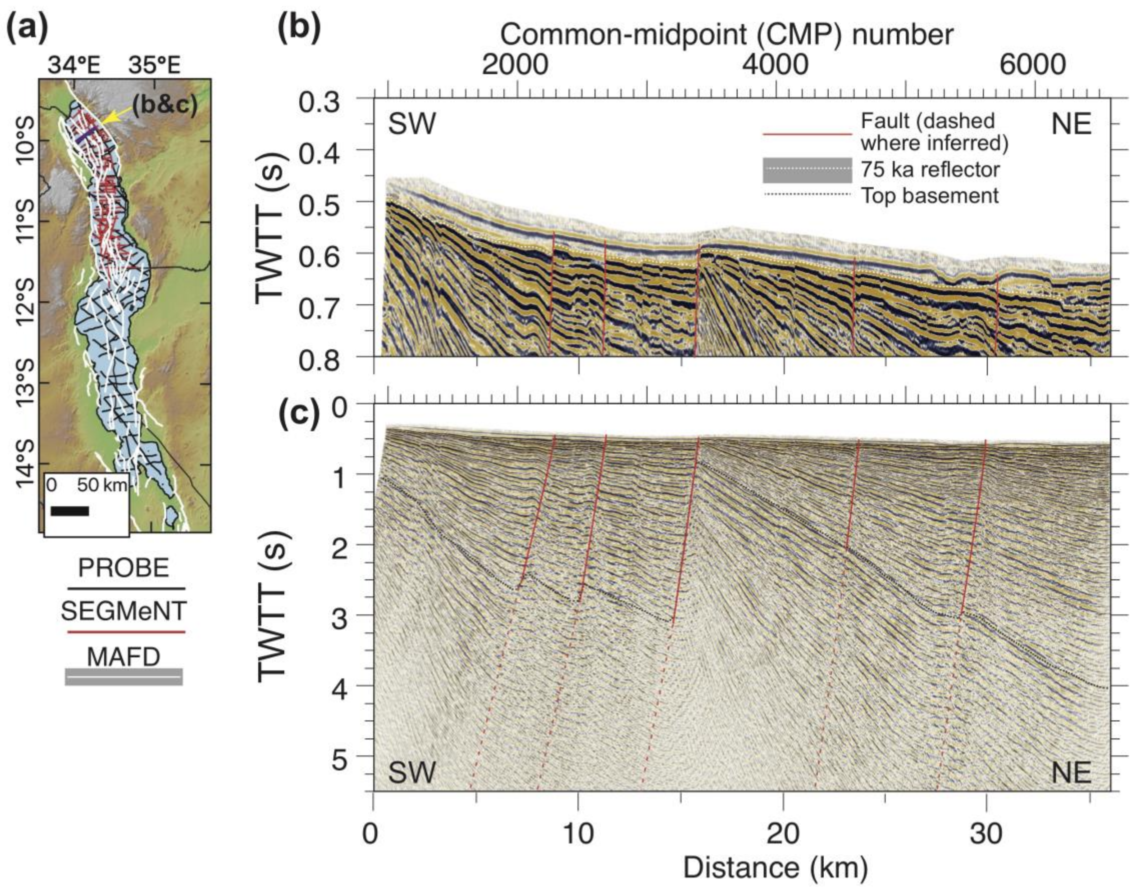

Figure 4: Seismic reflection data used for mapping offshore faults in the MAFD. (a) Track lines for Project PROBE and SEGMeNT surveys in Lake Malawi [*Scholz et al.*, 2020; *Shillington et al.*, 2016, 2020]. (b&c) Example of SEGMeNT multichannel seismic reflection data from the North Basin of Malawi taken parallel to dip direction (see (a)). In (b) offsets on young sediments including 75 Ka reflector are highlighted, whilst (c) demonstrates full thickness of EAR sediments and basement.

Figure 5

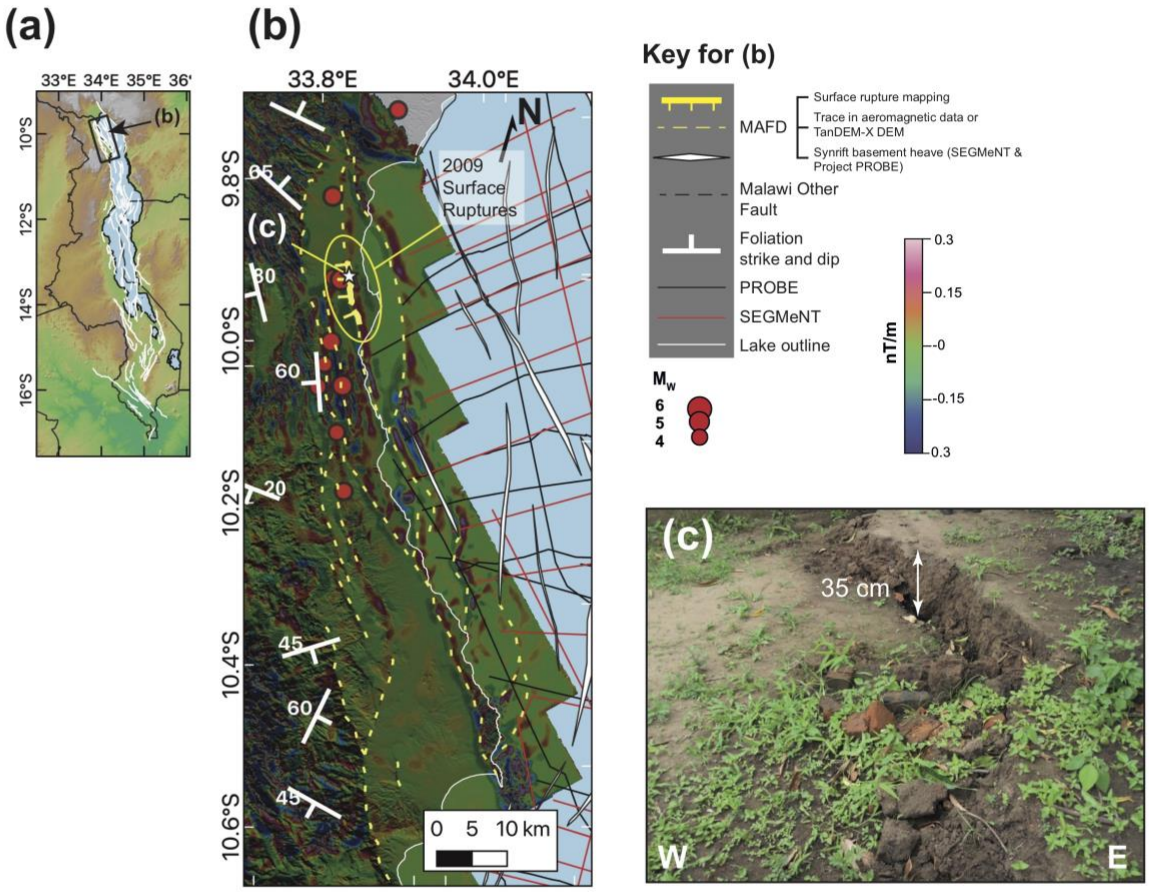

Figure 5: Use of aeromagnetic data and seismic reflection surveys to identify onshore to offshore active faults in northern Malawi [*Kolawole et al.*, 2018a; *Scholz et al.*, 2020; *Shillington et al.*, 2020]. (a) Location map. (b) Active fault map with synrift basement heaves mapped from seismic reflection surveys [white polygons; *Scholz et al.*, 2020], and their extrapolation using offshore aeromagnetic data in yellow. Foliation orientation surface measurements [*Kemp*, 1975; *Ray*, 1975; *Thatcher*, 1975], and 2009 Karonga Earthquake sequence surface ruptures [*Kolawole et al.*, 2018a; *Macheyeki et al.*, 2015] and global Centroid Moment Tensor (CMT) catalog earthquake locations [*Ekström et al.*, 2012; *Gaherty et al.*, 2019] also shown. Map underlain by aeromagnetic image created from the first vertical derivative of the 2013 aeromagnetic grid [*Kolawole et al.*, 2018a], and TanDEM-X 12

m DEM. (c) Surface rupture along the St Mary fault following the 2009 Karonga earthquake sequence.

Figure 6

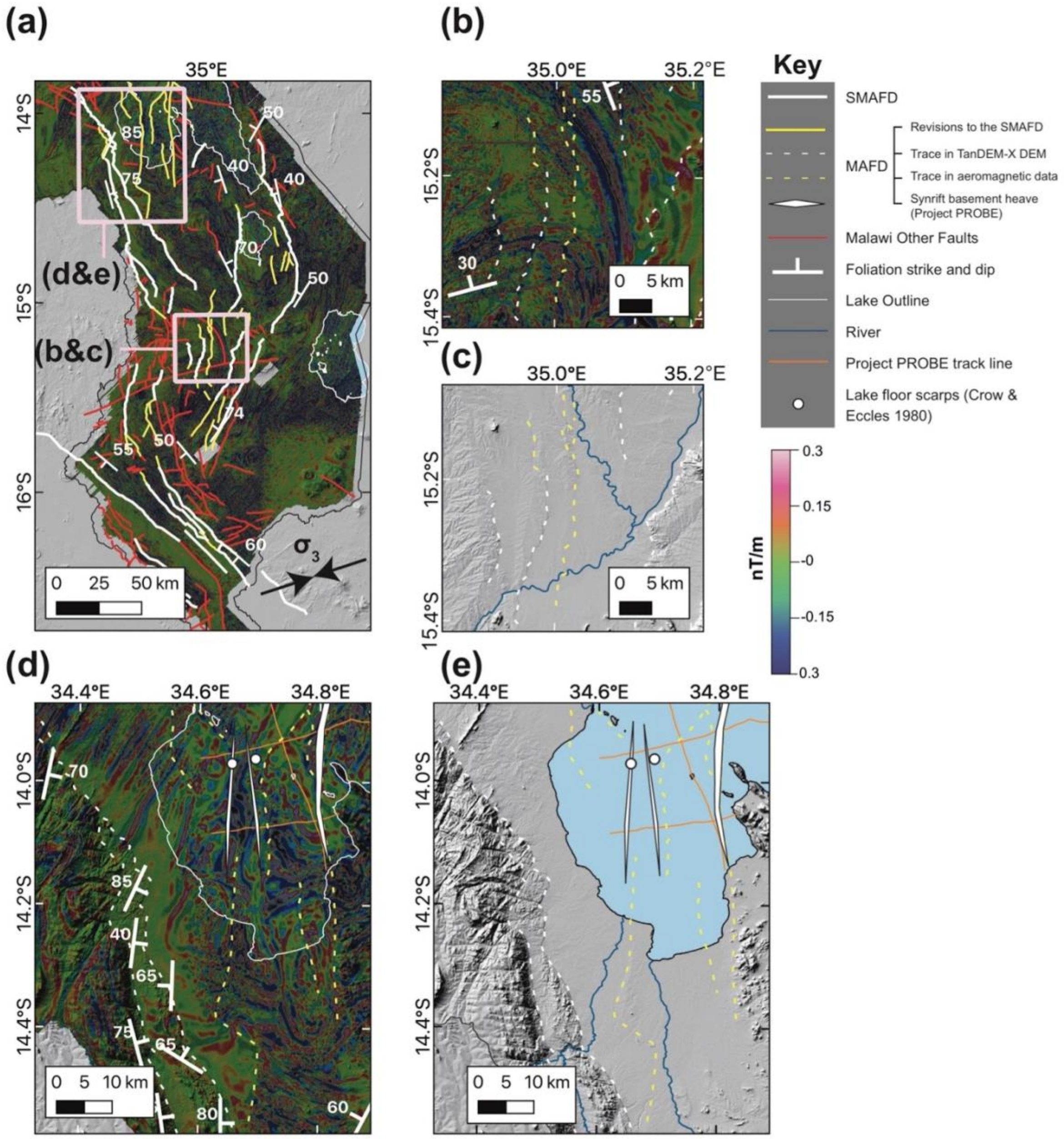

Figure 6: Use of aeromagnetic data and TanDEM-X DEM's to identify and map faults in southern Malawi. (a) The South Malawi Active Fault Database [SMAFD; *Williams et al.*, 2021] in comparison to the updated fault mapping in the Malawi Active Fault Database (MAFD) following the use of aeromagnetic data to revise the length of previously mapped faults and to identify faults with no surface expression [*Kolawole*

et al., 2021]. Revised and newly identified faults in the MAFD highlighted in yellow. Map underlain by TanDEM-X 12 m resolution DEM, vertical derivative of 2013 aeromagnetic grid, and surface measurements of foliation [*Bloomfield*, 1958; *Bloomfield & Garson*, 1965; *Dawson & Kirkpatrick*, 1968; *Habgood et al.*, 1973; *Walshaw*, 1965]. The ‘Malawi Other Faults’ database, which represents faults in Malawi that have no evidence for EAR activity or are misoriented with respect to the regional minimum principal compressive stress trend [σ_3; *Williams et al.*, 2019] are also shown. Examples of active faults in the MAFD from (b&c) the Zomba Graben and (d&e) Makanjira Graben and southwestern arm of Lake Malawi. In both examples, maps are shown with and without aeromagnetic data to highlight the faults in the MAFD that have and do not have a surface expression.

Figure 7

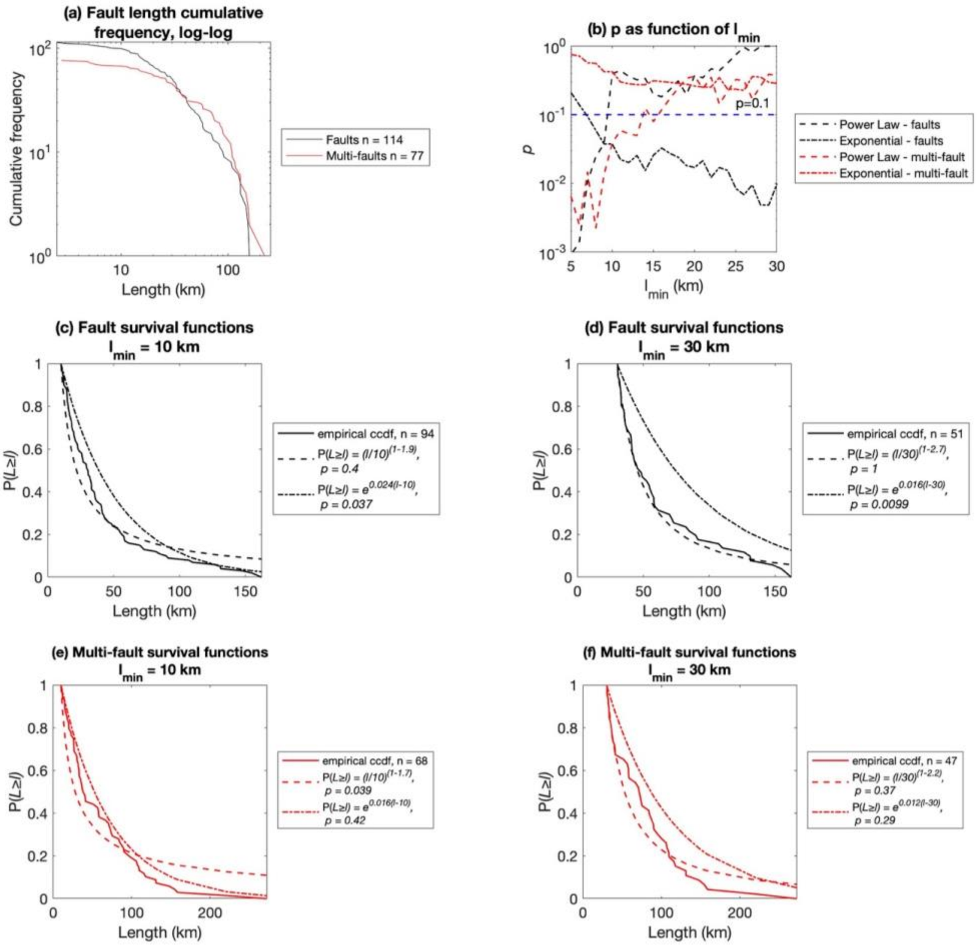

Figure 7: Analyses of fault length distributions in the MAFD. (a) The empirical cumulative frequency of the lengths of all faults documented in the Malawi Active Fault Database (MAFD). This plot considers cases where each fault in the MAFD represents a distinct fault, and where closely spaced en-echelon faults represent a single structure (the ‘multi-fault case’). (b) Results from two sample Kolmogorov-Smirnov (K-S) tests for the fit between empirical and theoretical survival functions of fault lengths in the MAFD, for lower bounds of fault length (l_{min}) between 5-30 km. Both power-law (equation 1) and exponential (equation 2) survival functions are considered in the K-S tests, with the power-law exponent and exponential rate

parameter estimated via maximum likelihood. The value of p (0.1) below which the K-S test rejects the null hypothesis is also highlighted. (c&d) Empirical and theoretical survival functions of fault lengths in the MAFD for representative values of l_{min} of 10 and 30 km, and assuming that each fault represents a distinct structure. The equation for the theoretical trend, and its fit to the empirical trend (i.e., the p-value from a K-S test), is also reported. (e&f) Equivalent to c&d, but assuming the multi-fault case.

Figure 8

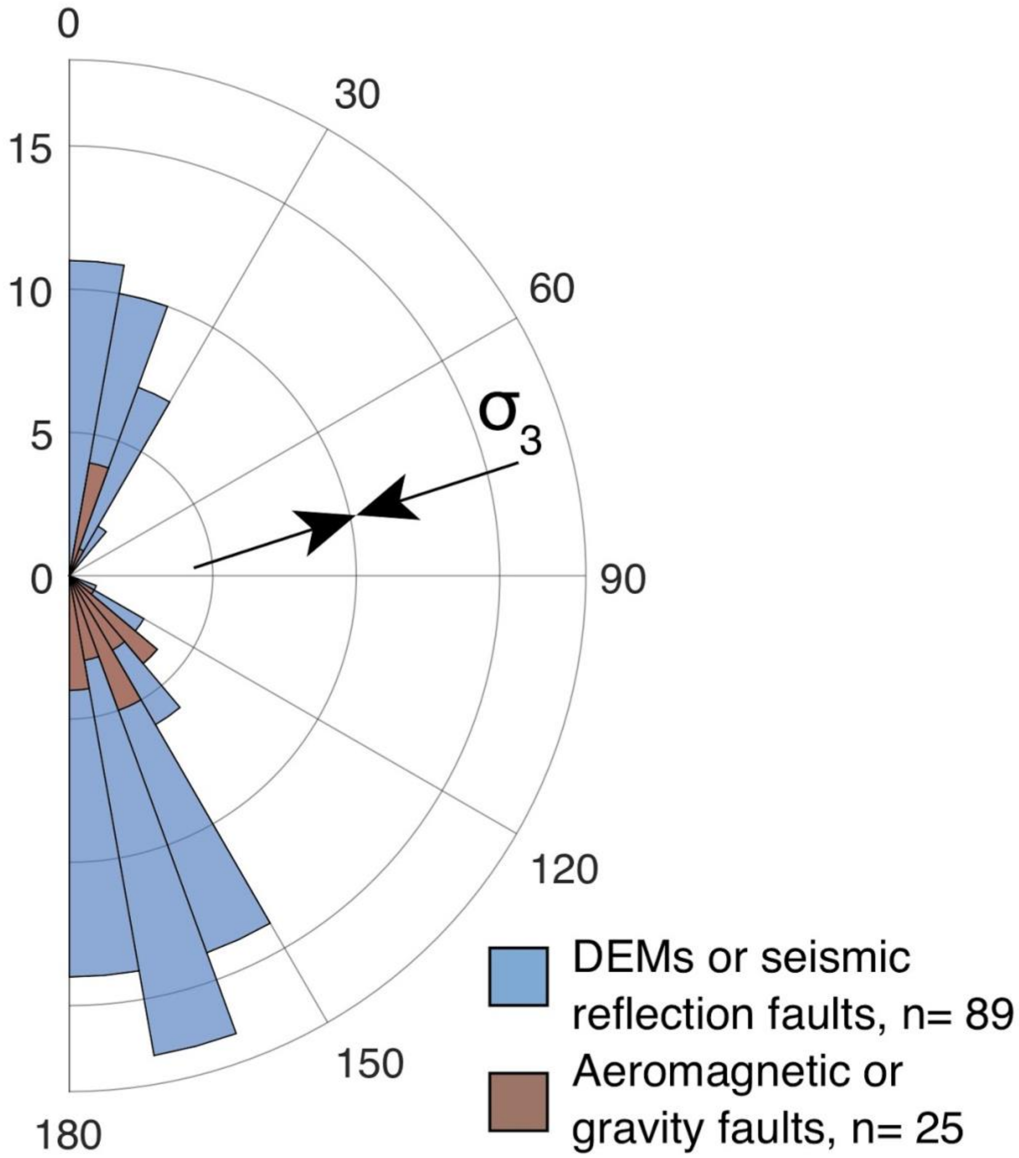

Figure 8: Rose plot depicting the distribution of fault strike in the MAFD with respect to the trend of the minimum principal compressive stress (σ_3) in Malawi derived from an earthquake focal mechanism stress inversion [*Williams et al.*, 2019]. Faults identified from aeromagnetic or gravity data are indicated separately, as their inclusion in the MAFD is dependent on their orientation with respect to σ_3.